Antisense PMO Found in Dystrophic Dog Model Was Effective in Cells from Exon 7-Deleted DMD Patient

Takashi Saito[1,2], Akinori Nakamura[1], Yoshitsugu Aoki[1], Toshifumi Yokota[3], Takashi Okada[1], Makiko Osawa[2], Shin'ichi Takeda[1]*

1 Department of Molecular Therapy, National Institute of Neuroscience, National Center of Neurology and Psychiatry, Kodaira, Tokyo, Japan, **2** Department of Pediatrics, School of Medicine, Tokyo Women's Medical University, Shinjuku, Tokyo, Japan, **3** Research Center for Genetic Medicine, Children's National Medical Center, Washington, District of Columbia, United States of America

Abstract

Background: Antisense oligonucleotide-induced exon skipping is a promising approach for treatment of Duchenne muscular dystrophy (DMD). We have systemically administered an antisense phosphorodiamidate morpholino oligomer (PMO) targeting dystrophin exons 6 and 8 to a dog with canine X-linked muscular dystrophy in Japan ($CXMD_J$) lacking exon 7 and achieved recovery of dystrophin in skeletal muscle. To date, however, antisense chemical compounds used in DMD animal models have not been directly applied to a DMD patient having the same type of exon deletion. We recently identified a DMD patient with an exon 7 deletion and tried direct translation of the antisense PMO used in dog models to the DMD patient's cells.

Methodology/Principal Findings: We converted fibroblasts of $CXMD_J$ and the DMD patient to myotubes by FACS-aided MyoD transduction. Antisense PMOs targeting identical regions of dog and human dystrophin exons 6 and 8 were designed. These antisense PMOs were mixed and administered as a cocktail to either dog or human cells *in vitro*. In the $CXMD_J$ and human DMD cells, we observed a similar efficacy of skipping of exons 6 and 8 and a similar extent of dystrophin protein recovery. The accompanying skipping of exon 9, which did not alter the reading frame, was different between cells of these two species.

Conclusion/Significance: Antisense PMOs, the effectiveness of which has been demonstrated in a dog model, achieved multi-exon skipping of dystrophin gene on the FACS-aided MyoD-transduced fibroblasts from an exon 7-deleted DMD patient, suggesting the feasibility of systemic multi-exon skipping in humans.

Citation: Saito T, Nakamura A, Aoki Y, Yokota T, Okada T, et al. (2010) Antisense PMO Found in Dystrophic Dog Model Was Effective in Cells from Exon 7-Deleted DMD Patient. PLoS ONE 5(8): e12239. doi:10.1371/journal.pone.0012239

Editor: Antoni L. Andreu, Hospital Vall d'Hebron, Spain

Received May 7, 2010; **Accepted** July 21, 2010; **Published** August 18, 2010

Funding: This work was supported by the Health and Labour Sciences Research Grants for Translational Research from the Ministry of Health, Labour and Welfare of Japan (H19-Translational Research-003, H21-Translational Research-011, H21-Clinical Research-011). The funders had no role in study design, data collection and analysis, decision to publish, or preparation of the manuscript.

Competing Interests: The authors have declared that no competing interests exist.

* E-mail: takeda@ncnp.go.jp

Introduction

Antisense oligonucleotides (AON) have been reported to modulate splicing of pre-mRNA transcribed from mutated genes and to restore a normal reading frame in several diseases. Duchenne muscular dystrophy (DMD), a degenerative muscle disorder caused mainly by nonsense or frame-shift mutations of the dystrophin gene, is one of the diseases that could be treated by AON-mediated exon skipping. Previously reported studies were conducted *in vitro*, in animal models, and as patient intervention studies, and they showed restorations of the reading frame in dystrophin mRNA and recoveries of dystrophin protein expression [1,2,3]. Among the several AON chemistries that have been introduced thus far, a phosphorodiamidate morpholino oligomer (PMO) and 2'-O-methyl phosphorothioate (2'OMe) oligomer are promising candidates owing to their stabilities and efficacies, and they are now undergoing phase I-II clinical trials in the United Kingdom and the Netherlands, respectively [4,5]. The AON-mediated exon skipping is already in a late early stage of clinical application; therefore, it is rational to translate pre-clinical animal model knowledge into a patient-based study.

We have previously reported that the systemic administration of an antisense PMO for canine X-linked muscular dystrophy in Japan ($CXMD_J$) achieved restoration of dystrophin and amelioration of symptoms [6]. $CXMD_J$ harbors a splice site mutation within the splice acceptor site of intron 6 of the dystrophin gene. The mutation disrupts the splicing of exon 7, and thus the dystrophin mRNA lacks exon 7 [7]. In $CXMD_J$, multiple skipping of exons 6 and 8 restores the reading frame, and the multi-exon skipping approach is expected to expand the number of DMD cases potentially treatable by exon skipping [8]. $CXMD_J$ is an ideal model of multi-exon skipping, and we hope to translate the results to human patients. However, in the road to ongoing clinical trials, *in vitro* assays on patient cells are indispensable.

To date, antisense sequences used for exon skipping in DMD animal models have not been directly applied to a DMD patient having the same type of exon deletion. We identified an exon 7-deleted patient (referred to as DMD 8772) and tried direct

translation of the antisense PMO design from a DMD dog model to the DMD patient. We tried *in vitro* multi-exon skipping with the same antisense PMO that was used in $CXMD_J$ in the patient's cells before attempting delivery of the PMO into the patient.

Which cells should be used for *in vitro* dystrophin exon skipping is controversial. Myoblasts are usually employed simply because they express enough dystrophin as mRNA and protein, but collecting them requires an invasive muscle biopsy. In cases where myoblasts were not available, it had been reported that the dystrophin mRNA was detected in lymphocytes and fibroblasts by nested RT-PCR. Some studies actually demonstrated the success of exon skipping in mRNA of lymphoblastoid cells and fibroblasts [9,10], but the restoration of dystrophin protein could not be analyzed in these cells because their transcripts were illegitimate and too low to be translated into gene products [11]. As another alternative, fibroblasts are converted to myotubes by MyoD transduction [4,12,13]. Transduced cells express dystrophin mRNA and protein, but achievement of sufficient protein expression is challenging [14,15,16]. In this study, we addressed this issue by introducing a retroviral vector co-expressing MyoD and green fluorescent protein (GFP) and flow cytometry, and then quantified the dystrophin expression of the cells to evaluate the feasibility of exon skipping.

We first report multiple skipping of dystrophin exons 6 and 8 in the DMD patient's cells and translation of the unified antisense PMO design from a DMD dog model to a human based on the MyoD-transduction method utilizing flow cytometry.

Results

Mutation analysis of DMD 8772

DMD 8772, a 22-year-old man, manifested severe muscle weakness, wheelchair dependency, and mild cardiac dysfunction. No evidence of dystrophin protein had been observed on a previous muscle biopsy, and the patient had been diagnosed with a frame-shift deletion of dystrophin exon 7 by multiplex ligation-dependent probe amplification (MLPA) analysis. The deletion of exon 7 leads to a premature translation termination at exon 8. The deletion of exon 9 is known as a common splice variant maintaining the reading frame in dogs and humans [17,18] (**Figure 1A**). RT-PCR analysis of dystrophin mRNA using the patient's lymphocytes showed an exon 7 deletion, and direct sequence analysis of the RT-PCR products revealed a conjunction of exons 6 and 8 (**Figure 1B**). To determine the intron length, we performed a deletion breakpoint analysis. The genomic PCR roughly narrowed the breakpoint window to 2.5 kb between introns 6 and 7, then primer walking sequence analysis revealed the 50.4 kb deletion (Vega v35 chromosome X 32771568 to 32821979) [13] and the breakpoint accompanying an insertion of 13 bases of unknown origin (**Figure 1C**).

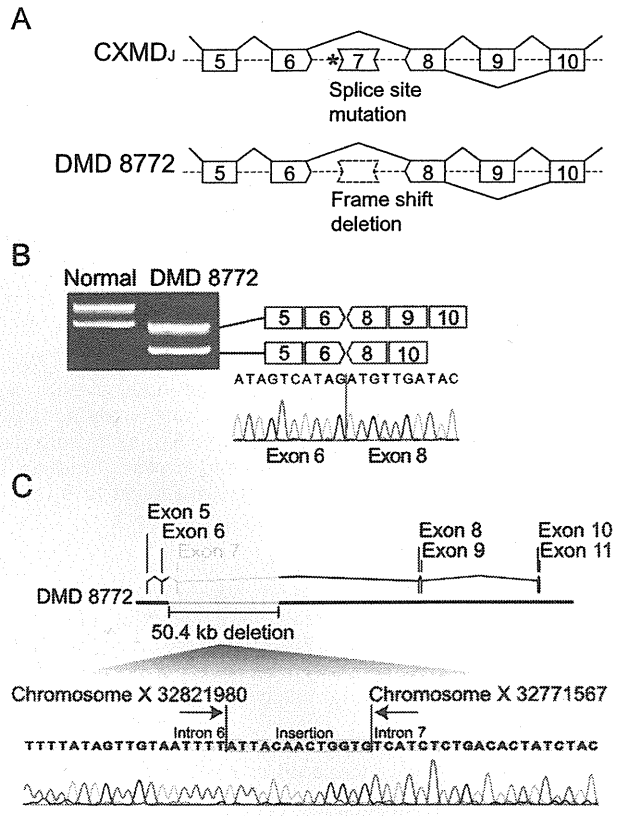

Figure 1. Mutation analysis of DMD 8772. (A) Splice-site mutation of a splice acceptor site in intron 6 (asterisk) excludes exon 7 from dog dystrophin mRNA. Frame-shift deletion of dystrophin exon 7 in DMD 8772 was diagnosed by MLPA analysis. Skipping of exon 9 is a frequent splice variant. Both ends of the schematic box of the exon represent a phase of the codon (see detail, Yokota et al. 2009). (B) RT-PCR and sequence analysis of dystrophin mRNA using normal and DMD 8772 lymphocytes. Double bands due to a splicing variant of exon 9 were observed. (C) Breakpoint analysis of DMD 8772 revealed a 50.4 kb deletion from intron 6 to intron 7, and the insertion of 13 bases of unknown origin.
doi:10.1371/journal.pone.0012239.g001

Myogenic conversion of fibroblasts by MyoD transduction and selection of appropriate cell lineage for exon skipping

We prepared lymphoblastoid cells, fibroblasts, and MyoD-transduced fibroblasts from DMD 8772 and assessed the feasibility of exon skipping in these cells. To establish MyoD-transduced fibroblasts, primary fibroblasts were transfected by a retrovirus encoding murine or human MyoD and GFP with the vesicular stomatitis virus (VSV-G) envelope through standard procedures (**Figure 2A**) [19,20]. To compare exon skipping between corresponding cells of $CXMD_J$ and DMD 8772, fibroblasts from both were converted. In addition, normal dog and human fibroblasts were also transduced for evaluation. After virus transfection, we sorted GFP-positive cells by flow cytometry. The ratio of GFP-positive to -negative cells was dependent on cell lineage, and affected cells generally showed lower transfection efficiencies (**Figure 2B**). The GFP-positive cells were isolated in serum-deprived medium for myogenic differentiation and cultured for 10 to 16 days. We confirmed that the cultured cells had the morphological features of myotubes of multiple nuclei and longitudinal growth. Immunostaining analysis showed nuclear localization of MyoD and expressions of the muscle-specific proteins desmin, myosin heavy chain, and dystrophin (**Figure 2C**). Using normal dog and human fibroblasts, we performed time-course expression analyses of dystrophin mRNA by qRT-PCR and dystrophin protein by Western blot. The results showed a gradual increase in dystrophin expression. In dog cells, dystrophin became detectable on the protein level seven days after differentiation, whereas human cells required two weeks or more (**Figure 2D**). We compared the dystrophin mRNA expression of the lymphoblastoid cells, fibroblasts, and MyoD-transduced fibroblasts from DMD 8772. The MyoD-transduced fibroblasts showed remarkable expression compared with the other cells (**Figure 2E**). We tried exon skipping in lymphoblastoid cells, fibroblasts and MyoD-transduced fibroblasts, but only the MyoD-transduced

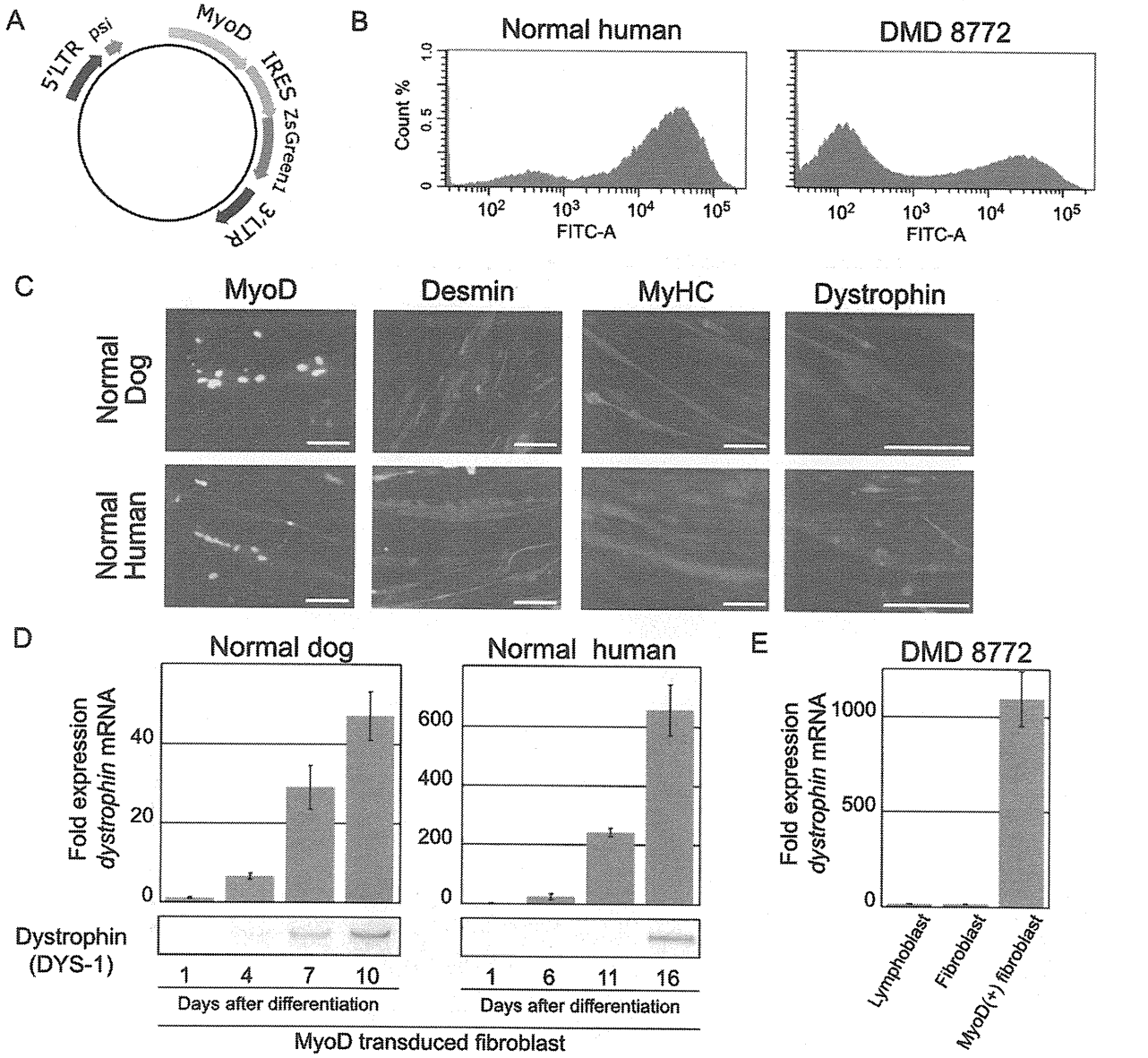

Figure 2. Myogenic conversion of fibroblasts and dystrophin expression. (A) Schematic diagram of the retroviral expression vector. (B) Histograms showing GFP fluorescence intensity compared with cell numbers of normal human and DMD 8772 MyoD-GFP-transduced fibroblasts. Both cells were analyzed five days after retroviral transfection. (C) Immunostaining of MyoD-transduced of dog and human fibroblasts after 10 and 15 days of myogenic differentiation, respectively. MyHC, myosin heavy chain. The nuclei were counter-stained with DAPI. Scale bar: 100 μm. (D) The time course of dystrophin expression in dog and human MyoD-transduced fibroblasts by qRT-PCR and immunoblotting analysis. The mRNA levels were normalized to *GAPDH* and expressed relative to the amount of the lowest one in each group. For immunoblotting, 5 μg of total protein was loaded into each lane. Error bars indicate standard deviation. (E) Determination of dystrophin mRNA expression in each cell type from DMD 8772 by qRT-PCR. MyoD-transduced fibroblasts were assayed 15 days after differentiation. Normalization and relative expression are the same as (D).
doi:10.1371/journal.pone.0012239.g002

fibroblasts yielded reproducible results. The lymphoblastoid cells and fibroblasts often failed to produce PCR products, and the skipped in-frame products were undetectable even if PCR products were generated (**data not shown**). Therefore, we used MyoD-transduced fibroblasts in the subsequent assays.

Antisense PMO sequence design

In a previous systemic dog study, we used three antisense sequences, Ex6A, Ex6B, and Ex8A, as three antisense PMO cocktails [6]. Because there were two base mismatches between dog and human Ex6B, hEx6B was newly designed on the identical region of Ex6B, modifying the mismatches of the human sequence. In the systemic study, we skipped exon 6 with a combination of Ex6A and Ex6B, and thus we tried same strategy for exon 8. We newly designed several antisense PMOs targeting exon 8 that were positioned on the identical sequence in dog and human considering the predicted *in silico* splice-enhancer motifs (**Figure 3A**). A preliminary assay of $CXMD_J$ cells showed that three sequences, Ex8G, Ex8I, and Ex8K, were effective. Therefore, the antisense combination for exon 8 contained an extra antisense sequence

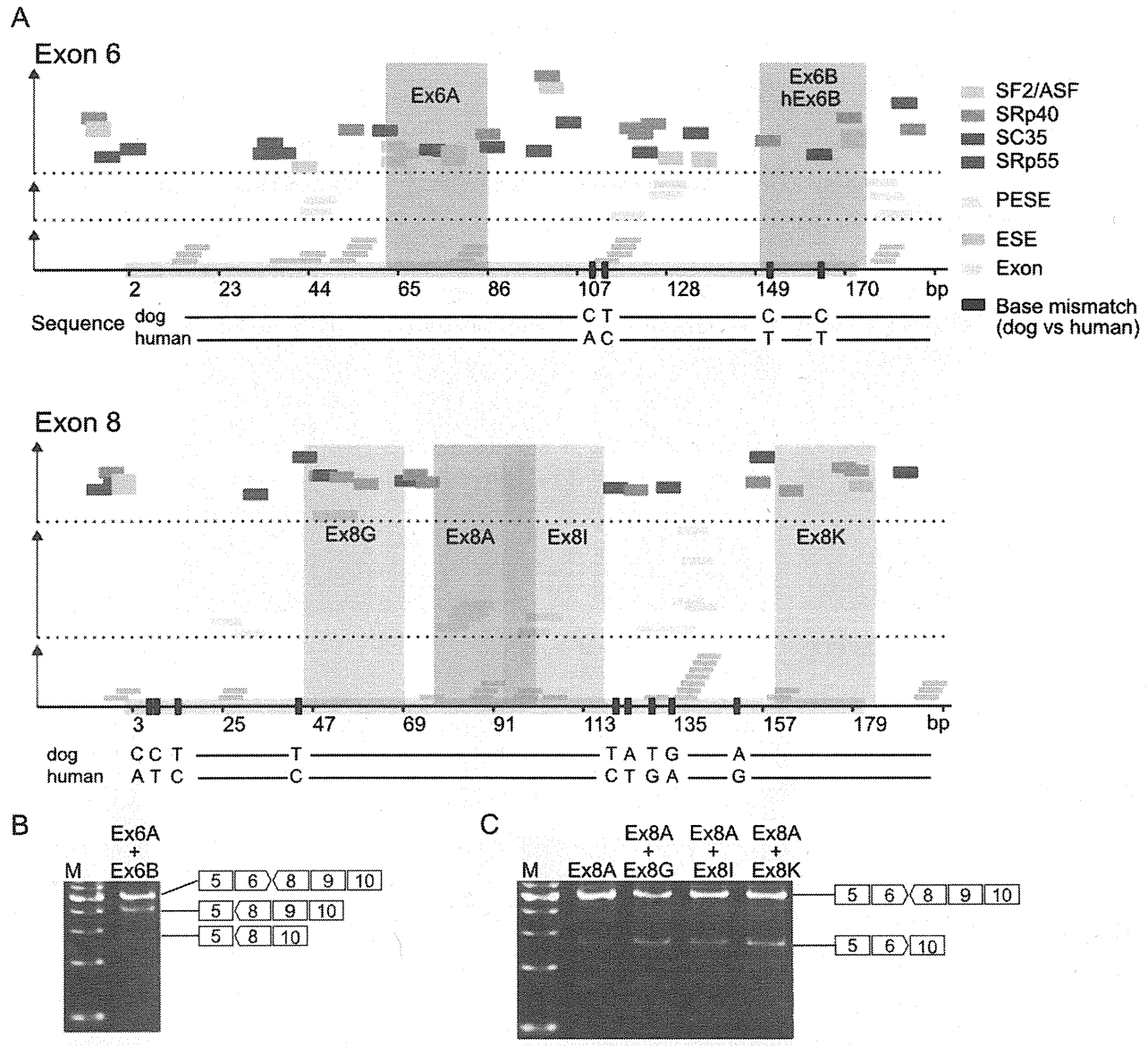

Figure 3. Design of antisense PMO sequence targeting exons 6 and 8. (A) Exonic splicing enhancer motifs predicted *in silico* based on human sequence (small coloured boxes) and positions of antisense PMOs (green and blue rectangular areas). The horizontal axis represents base positions in each exon from 5′ to 3′, and the vertical axis represents relative predicted values of the motifs. PESE: putative exonic splicing enhancer. ESE: exonic splicing enhancer. Base mismatches between dog and human (black bar) are indicated in the exon (grey box). RT-PCR of dystrophin mRNA of MyoD-transduced $CXMD_J$ fibroblasts treated with (B) a mixture of Ex6A and Ex6B and (C) only Ex8A or mixtures containing Ex8A.
doi:10.1371/journal.pone.0012239.g003

from Ex8G, Ex8I, or Ex8K in addition to that of Ex8A. The skipping efficacy of each combination was higher than that of Ex8A alone, and those of Ex8G, Ex8I, and Ex8K were comparable (**Figure 3C**).

Comparison of multiple skipping of exons 6 and 8 between $CXMD_J$ and DMD 8772 cells

The multi-exon skipping of exons 6 and 8 employed three- and four-antisense PMO cocktails. In the three-antisense PMO cocktail for dogs, Ex6A, Ex6B, and Ex8A were included, and Ex6B was replaced with hEx6B for the human. The four-antisense PMO cocktail included one of Ex8G, Ex8I, or Ex8K in addition to the three-antisense PMO cocktail (**Figure 4A**). When we transfected the three- or four-antisense PMO cocktails into the MyoD-transduced fibroblasts, we did not observe the skipped products (231 bp) of exons 6-8 on RT-PCR analyses of $CXMD_J$ but did observe the skipped products (99 bp) of exons 6-9. A sequence analysis also confirmed the concatenation of exons 5 and 10. In DMD 8772, we observed skipped products (221 bp and 92 bp, respectively) of both exons 6-8 and exons 6-9. Sequence analysis also showed that the skipped products were concatenations of exons 5 to 9 and exons 5 to 10. The four-PMO cocktails produced more in-frame products than the three-PMO cocktail, but we discerned no difference among the four PMO cocktails. This tendency was also consistent between $CXMD_J$ and DMD 8772 (**Figure 4B**). Immunostaining analysis showed partial recovery of dystrophin in the four-antisense PMO

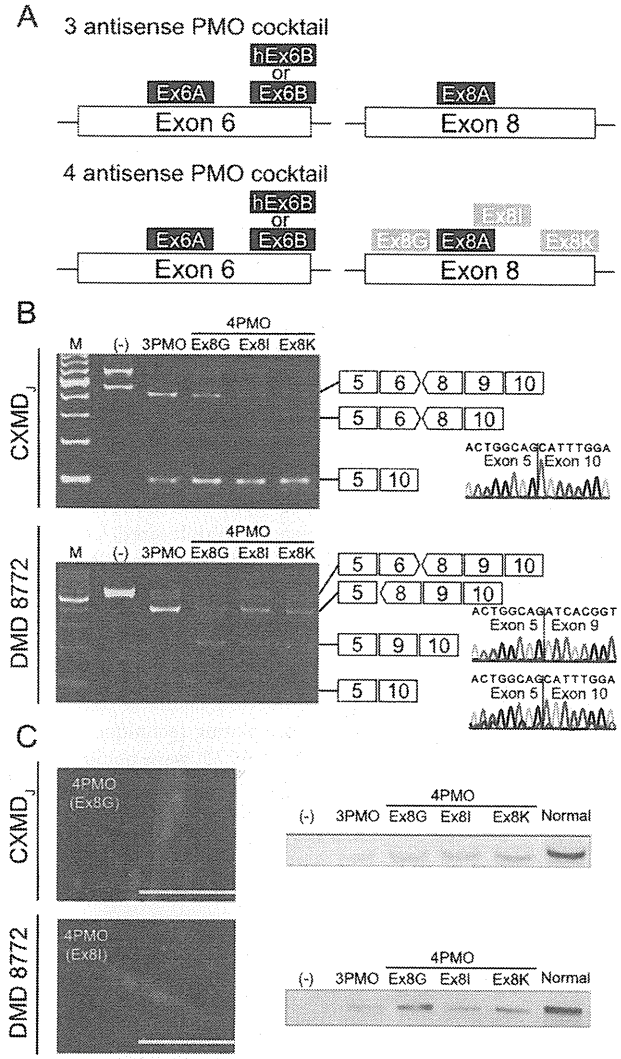

Figure 4. Multi exon skipping and recovery of dystrophin in CXMD$_J$ and DMD 8772-derived cells. (A) Schematic diagram of the three- and four-antisense PMO cocktails. For DMD 8772, Ex6B was replaced with hEx6B. In the four-antisense PMO cocktail, one additional sequence (Ex8G, Ex8I, or Ex8K) was added to the three-antisense PMO cocktail. (B) RT-PCR of dystrophin mRNA isolated from MyoD-transduced fibroblasts after treatment with the three- and four-antisense PMO cocktails. In-frame exon skipping products were 99 bp in dog and 221 bp and 92 bp in human. (C) Representative immunostaining and immunoblotting analysis of MyoD-transduced fibroblasts treated with antisense PMO cocktails. The nuclei were counterstained with DAPI. Scale bar: 100 μm. Expected molecular weights of truncated human dystrophin with exons 6–8 and exons 6–9 skipped are 18.3 kDa and 23.1 kDa, respectively, smaller than the full-length dystrophin.
doi:10.1371/journal.pone.0012239.g004

cocktail-treated cells without obvious differences between them (**Figure 4C**). Western blots of dystrophin showed products that were slightly smaller than the full-length dystrophin. In RT-PCR of DMD 8772, skipped mRNA of both exons 6-8 and 6-9 were detected; however, distinguishing the truncated dystrophins translated from these mRNA variants was impossible. Similar to the RT-PCR results, the dystrophin expression level was higher with a four-PMO cocktail than with the three-PMO cocktail. Differences between the four-PMO cocktails were also undetectable.

Discussion

In this study, we accomplished *in vitro* multi-exon skipping in a DMD patient carrying the same deletion as CXMD$_J$ by using the identical antisense PMO. We also addressed the efficient MyoD transduction of fibroblasts with FACS, and discuss the difference of the spliced exon associated with it with the frequency of alternative splicing.

FACS-aided MyoD transduction provided sufficient dystrophin expression

We evaluated the appropriateness of lymphoblastoid cells, fibroblasts, and MyoD-transduced fibroblasts as an alternative to myoblasts for exon-skipping assays. Lymphoblastoid cells and primary fibroblasts dystrophin mRNA required reamplification by nested RT-PCR [9,10], and the results were not reproducible, suggesting that low dystrophin expression may hamper reliable quantitative assessments. Only MyoD-transduced fibroblasts showed reproducible results due to their stable dystrophin expression. We employed flow cytometry for selection of MyoD-positive cells; it seems to offer several advantages against conventional drug-resistance selection. First, the transfection ratio in drug-resistance selection remains unknown until a selective drug is added. In contrast, with MyoD-transduced fibroblasts, we were able to roughly determine the ratio by fluorescence microscopy and adjust the culture scale to meet the size of the assay. Second, a low rate of myotubes formation after drug-resistance selection has been reported [21]. Our method actively selects MyoD-positive cells and enables pure clusters of MyoD-positive cells to form myotubes efficiently. MyoD transduction with GFP has been reported in several studies [22,23] but not in dystrophin exon-skipping studies. We demonstrated that it is a suitable approach for the exon-skipping assay here as well. Several studies have reported difficulties inducing dystrophin in human cells with MyoD transduction [14,15,16]. In our experience, the typical morphological features of myotubes, multiple nuclei and longitudinal cell growth, do not necessarily indicate sufficient dystrophin expression. Seeding MyoD-positive cells at high density ($>5.0\times10^4$ cells/cm^2) and incubating for longer periods (>2 weeks) were critical to induce sufficient dystrophin expression. Detachment of differentiated myotubes from culture wells was also problematic; supporting them with a coating matrix seems to promise better results.

Direct translation of antisense PMO from dog to human was feasible

We previously reported systemic multi-exon skipping in CXMD$_J$ with a 3-antisense PMO cocktail and amelioration of dystrophic pathology [6]. The effectiveness of the 3-antisense PMO cocktail was confirmed in MyoD-transduced fibroblasts derived from DMD 8772 as well. When the dog and human sequences were compared, 97% of dystrophin exon 6 and 95% of dystrophin exon 8 matched on the sequence level. This similarity enabled use of the unified antisense design methodology targeting the same sequence. We demonstrated that the identical antisense PMO sequence designed for dog and achieved multi-skipping of exons 6 and 8 in human cells. The skipping efficacies of the PMOs were indistinguishable between CXMD$_J$ and DMD 8772; the superior efficacy of the four-PMO cocktail against that of the three-PMO cocktail and the equivalent efficacies of each four-PMO cocktail were comparable. CXMD$_J$ shows more similarity in the pathogenic phenotype to human DMD than to *mdx* mice [24]. These findings imply that not only the similarity in the sequence but also the similarity in the pathogenic phenotype contributed to the comparable results.

No study has yet compared the exon skipping due to identical antisense PMOs between cells of different species carrying same exon deletion in mRNA. Recent investigations have reported a limitation in designing efficient antisenses to induce human dystrophin skipping in a mice model assay [25]; however, we confirmed the feasibility of direct translation of an antisense PMO from a DMD dog model to a DMD patient, at least *in vitro*, for the first time.

The four-antisense PMO cocktail, the addition of a fourth antisense sequence to the three-antisense PMO cocktail, increased the efficiency of skipping as previously reported [26,27]. The effectiveness of the four-antisense PMO cocktails, however, must be evaluated *in vivo*, and we are planning systemic treatment of $CXMD_J$ with them. Our results underscore the usefulness of $CXMD_J$ as a DMD model for translational research and advance the prospect that systemic treatment of the DMD patient by multi-exon skipping is possible.

Mode of exon 9 skipping might be affected by frequency of alternative splicing

With the antisense PMO targeting exons 6 and 8, exon 9 was always skipped in $CXMD_J$, although it was only partially skipped in DMD 8772. Two possibilities were considered to explain the difference: (1) the effects of the shortened introns 6 and 7 due to the deletion around exon 7 in DMD 8772 (**Figure 5**), and (2) the different frequencies of alternative splicing of exon 9. For the former case, we tried exon 8 skipping using a combination of Ex8A and Ex8G in normal and affected human MyoD-transduced fibroblasts, and found that the skipping of exon 8 and exons 8/9 happened simultaneously (**Figure S1**). Therefore, it is unlikely that the intron length affects the difference. In the latter case, the untreated MyoD-transduced fibroblasts from $CXMD_J$ clearly showed one normal and one alternative transcript; on the other hand, the untreated sample from DMD 8772 showed only a normal transcript, suggesting that the frequency of alternative splicing of exon 9 is an underlying factor in the difference. It was reported that an antisense oligonucleotide targeting exon 8 facilitates the skipping of exon 9 as well as exon 8 by effecting the concatenation of exons 8 and 9 in human and dog cells [28].

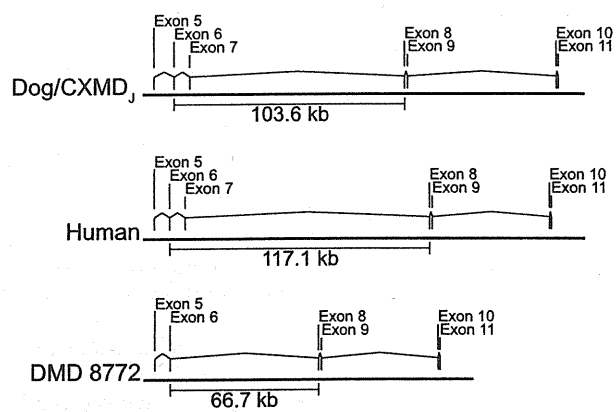

Figure 5. Location of dystrophin exons 5 to 11 in the genome. Distances from dystrophin exon 6 to exon 8 are indicated based on the GenBank reference sequences of *Canis familiaris* chromosome X genomic contig, whole genome shotgun sequence (NW_879562.1) and *Homo sapiens* 211000035840903 genomic scaffold, whole genome shotgun sequence (CH471074.1).
doi:10.1371/journal.pone.0012239.g005

These findings were observed in myoblasts but not in MyoD-tansduced fibroblasts [29,30,31]. As is well known, the mode of alternative splicing differs among various tissues [32,33], and our MyoD-transduced fibroblasts might have characteristics that are incompatible with the alternative splicing of exon 9.

In summary, MyoD transduction of fibroblasts with the help of FACS may be practical for exon skipping assays, and the direct translation of an antisense PMO from a DMD dog model to a DMD patient was feasible *in vitro*, suggesting that the animal model-based antisense PMO for multiple skipping could be effective for humans as well.

Materials and Methods

Ethics Statement

The patient samples were collected and used with the approval of the Ethics Committee of the National Center of Neurology and Psychiatry, approval ID: 20-4-6. Written informed consent was obtained from the donor. The dog study was approved by the Ethics Committee for the Treatment of Middle-sized Laboratory Animals of the National Center of Neurology and Psychiatry, approval ID: 20-05.

Cell culture

Dog primary myoblasts and fibroblasts were obtained from muscle specimens of normal and affected neonatal dogs of the $CXMD_J$ colony using a standard pre-plating technique. Primary fibroblasts of the DMD patient (DMD 8772) were obtained from skin explants and peripheral blood lymphocytes using Lymphocyte Separating Medium (PAN Biotech GmbH, Aidenbach, Germany). Lymphoblastoid cell lines were established by transformation with Epstein-Barr virus. The normal human fibroblast cell line TIG-119 was obtained from the Health Science Research Resource Bank (Osaka, Japan). Fibroblasts were cultured in 20% or 10% growth medium containing DMEM/F-12 1:1 (Invitrogen, San Diego, CA, USA), 20% or 10% fetal bovine serum, and 1% penicillin/streptomycin. For differentiation to myotubes, FACS-sorted MyoD-transduced fibroblasts were cultured in 2% differentiation medium containing DMEM/F-12 1:1, 2% horse serum, ITS Liquid Media Supplement (Sigma-Aldrich, St. Louis, MO, USA), and 1% penicillin/streptomycin.

Genomic mutation analysis

The dystrophin exon 7-deletion of DMD 8772 had been identified previously by MLPA. For breakpoint detection, lymphocyte genomic DNA was used as a template. Seven pairs of intron-spanning primers, positioned in the intron 6/7, were designed to yield 150-600 bp PCR products. A failure of PCR indicated deletions spanning the primer annealing sites. Four of seven primer pairs showed no amplification, suggesting that the deletion was more than 3.5 kb and less than 64.4 kb. Additionally, two intron 6 sense-primers and eight intron 7 antisense-primers were designed. Each primer pair was placed by flanking the breakpoint and expected to yield PCR products within the range of 4–64 kb. Primer sequences are available on request. PCR was performed using Phusion Hot Start High-Fidelity DNA Polymerase (Finnzymes, Keilaranta, Finland), and the cycling program was set to yield 16 kb products with a program of 35 cycles of 98°C for 10 sec, 60°C for 30 sec, and 72°C for 450 sec. Failure of PCR indicated products of more than 16 kb in size or the deletion of annealing sites. The breakpoint region was thus narrowed down to 2.5 kb, then primer walk sequencing was performed (Operon Biotechnologies, Tokyo, Japan).

MyoD transduction and cell sorting by FACS

The coding sequences of mouse *Myod1* (CCDS 21277.1) and human *MYOD1* (CCDS 7826.1) were derived from the Consensus CDS database [34]. The sequences were synthesized and cloned into a pUC57 vector (GenScript, Piscataway, NJ, USA). We subcloned it into a pRetroX-IRES-ZsGreen1 expression vector (Clontech, Mountain View, CA, USA). The expression vector, a pVSV-G envelope vector, and a gap-pol expression vector were co-transfected into a 293T packaging cell line using the standard calcium phosphate method. After 48–72 h incubation, the viral supernatant was collected and stored at −80°C. For retroviral transduction, the fibroblasts were harvested at 70–80% confluence in a T225 flask, and 2.5 ml thawed retroviral stock was added to 35 ml of growth medium. We added polybrene (Sigma-Aldrich) to a final concentration of 8 μg/ml. After 48–72 h incubation at 32°C, the culture medium was replaced with fresh growth medium, the cells were incubated at 37°C 1–3 d more, until the GFP-positive cells exceeded approximately 60%. Cell sorting was performed on a FACS VantageSE or FACSAria flow cytometry system (BD Bioscience, Franklin Lakes, NJ, USA). The recovered GFP-positive cells were seeded in Matrigel (BD Bioscience)-coated well plates at density of 5×10^4 cell/cm^2. After confirmation of cell attachment, the culture medium was changed to 2% differentiation medium. We cultured MyoD-transduced fibroblasts for 10 to 16 d to differentiate to myotubes.

Antisense PMO design and transfection to cultured cells

The antisense PMO sequences Ex6A, Ex6B, and Ex8A were described in Yokota et al. [6]. In addition, extra sequences hEx6B, Ex8G, Ex8I, and Ex8K were designed and synthesized (Gene Tools, LLC, Philomath, OR, USA). We used the Human Splicing Finder for *in silico* prediction of the splice-enhancer motifs [35]. All sequences are shown in **Table S1**. We transfected the antisense PMOs into myotubes differentiated from MyoD-transduced fibroblasts with a transfection agent, Endo-Porter (Gene Tools). In the 2% differentiation medium, the final concentration of the antisense PMO was 10 μM for a single sequence, 20 μM for two sequences, and a total of 30 μM for three or four sequences. A final concentration of Endo-Porter was 6 μM. After 48–72 h incubation with the PMO, the medium was changed to a fresh culture medium free of PMOs. The cells were recovered for analysis after 24–48 h in the PMO-deprived medium to allow sufficient time to translate dystrophin protein.

Quantitative RT-PCR analysis

Total RNA was extracted from MyoD-transduced fibroblasts obtained from normal subjects using Trizol (Invitrogen) at the time points specified. Total RNA (100-200 ng) was employed for cDNA synthesis using a QuantiTect Reverse Transcription Kit (Qiagen, Hilden, Germany). Quantitative real-time PCR was performed using ExTaq II SYBR (Takara, Kyoto, Japan) and a MyiQ Single-Color Real-Time PCR detection system (Bio-Rad, Hercules, CA). Primer sequences are shown in **Table S2**. Expression of dystrophin mRNA was normalized to *GAPDH* mRNA, and the time course of the increment was calculated by the delta-delta-Ct method.

RT-PCR and sequence analysis

As well as quantitative RT-PCR analysis, total RNA extraction and cDNA synthesis were performed. For myoblasts and MyoD-transduced fibroblasts, 35 cycles of denaturing at 98°C for 10 sec, annealing at 63°C for 30 sec, and extension at 72°C for 1 min were performed with ExTaq DNA polymerase (Takara). For fibroblasts and lymphoblasts, nested PCR was performed. Primer sequences are shown in **Table S3**. PCR products were electrophoresed on 1.2% SeaKem LE agarose gel (Lonza, Basel, Switzerland). The bands of interests were excised using a Wizard SV Gel and PCR Clean-Up system (Promega, Fitchburg, WI, USA), then sequenced directly or cloned into a vector using a TOPO-TA Cloning Kit (Invitrogen) with standard cloning techniques. Sequencing was performed by Fasmac Corporation (Kanagawa, Japan).

Immunostaining analysis

Cells were fixed in 3% paraformaldehyde, permeabilized in 10% Triton-X, then blocked by 10% goat serum in PBS for 1 h at room temperature. The cells were incubated with the primary antibody for 1 h at room temperature using anti-dystrophin (NCL-Dys1, diluted 1:30, Novocastra, Newcastle upon Tyne, UK), anti-myosin heavy chain (NCL-MHCf, diluted 1:30, Novocastra), anti-MyoD (NCL-MyoD1, diluted 1:30, Novocastra), or anti-desmin (NCL-DES-DERII, diluted 1:30, Novocastra). Incubation with the secondary antibody was performed for 30 min at room temperature using anti-rabbit or anti-mouse IgG (Alexa Fluor 546 highly cross-adsorbed, diluted 1:300, Invitrogen). Antibodies were diluted in Can Get Signal Immunostain A solution (Toyobo, Osaka, Japan). To visualize nuclei and enhance fluorescence signals, cells were mounted with Pro Long Gold Antifade reagent (Invitrogen).

Immunoblotting analysis

Protein was extracted from cultured cells using RIPA buffer (Thermo Fisher Scientific, Rockford, IL, USA) containing Complete Mini (Roche Applied Science, Indianapolis, IN, USA) as a protease inhibitor. Protein concentrations were determined using a BCA protein assay kit (Thermo Fisher Scientific) and equalized. After being mixed with an equal volume of EzApply sample buffer (ATTO Corporation, Tokyo, Japan), cell lysates containing equal amounts of total protein were denatured at 95°C for 5 min, electrophoresed in NuPAGE Novex Tris-Acetate Gel 3–8% (Invitrogen) at 150 V for 75 min, and transferred onto an Immobilon-P membrane (Millipore Corp., Billerica, MA, USA). Membranes were blocked for 1 h with 5% ECL Blocking agent (GE Healthcare, Buckinghamshire, UK) and probed with anti-dystrophin antibody (NCL-Dys1, diluted 1:50, Novocastra), followed by incubation with peroxidase-conjugated goat-anti-mouse IgG (Bio-Rad). An ECL Plus Western blotting system (GE Healthcare) was used to detect protein bands.

Supporting Information

Figure S1 RT-PCR of dystrophin mRNA isolated from the normal and affected human MyoD-transduced fibroblasts after the single exon 8 skipping.
Found at: doi:10.1371/journal.pone.0012239.s001 (0.30 MB PDF)

Table S1 Sequences of antisense PMO for dystrophin gene (for dog and human if not specified).
Found at: doi:10.1371/journal.pone.0012239.s002 (0.07 MB PDF)

Table S2 Sequences of qRT-PCR primers.
Found at: doi:10.1371/journal.pone.0012239.s003 (0.07 MB PDF)

Table S3 Sequences of RT-PCR primers.
Found at: doi:10.1371/journal.pone.0012239.s004 (0.07 MB PDF)

Acknowledgments

The authors thank Yu-ichi Goto (Department of Mental Retardation and Birth Defect Research, National Center of Neurology and Psychiatry), Narihiro Minami (Department of Neuromuscular Research, National Center of Neurology and Psychiatry), Hirofumi Komaki (Department of Child Neurology, National Center of Neurology and Psychiatry), Katsutoshi Yuasa (Research Institute of Pharmaceutical Sciences, Faculty of Pharmacy, Musashino University, Tokyo, Japan), and Tetsuya Nagata, Yuko Shimizu, and Satoru Masuda (Department of Molecular Therapy, National Center of Neurology and Psychiatry) for useful discussions and technical assistance.

Author Contributions

Conceived and designed the experiments: TS AN ST. Performed the experiments: TS YA. Analyzed the data: TS MO. Contributed reagents/materials/analysis tools: TY TO. Wrote the paper: TS AN ST.

References

1. Aartsma-Rus A, Bremmer-Bout M, Janson AA, den Dunnen JT, van Ommen GJ, et al. (2002) Targeted exon skipping as a potential gene correction therapy for Duchenne muscular dystrophy. Neuromuscul Disord 12(Suppl 1): S71–77.
2. Mann C, Honeyman K, Cheng A, Ly T, Lloyd F, et al. (2001) Antisense-induced exon skipping and synthesis of dystrophin in the mdx mouse. Proc Natl Acad Sci U S A 98: 42–47.
3. Alter J, Lou F, Rabinowitz A, Yin H, Rosenfeld J, et al. (2006) Systemic delivery of morpholino oligonucleotide restores dystrophin expression bodywide and improves dystrophic pathology. Nat Med 12: 175–177.
4. van Deutekom J, Janson A, Ginjaar I, Frankhuizen W, Aartsma-Rus A, et al. (2007) Local dystrophin restoration with antisense oligonucleotide PRO051. N Engl J Med 357: 2677–2686.
5. Kinali M, Arechavala-Gomeza V, Feng L, Cirak S, Hunt D, et al. (2009) Local restoration of dystrophin expression with the morpholino oligomer AVI-4658 in Duchenne muscular dystrophy: a single-blind, placebo-controlled, dose-escalation, proof-of-concept study. Lancet Neurol 8: 918–928.
6. Yokota T, Lu Q, Partridge T, Kobayashi M, Nakamura A, et al. (2009) Efficacy of systemic morpholino exon-skipping in Duchenne dystrophy dogs. Ann Neurol 65: 667–676.
7. Sharp N, Kornegay J, Van Camp S, Herbstreith M, Secore S, et al. (1992) An error in dystrophin mRNA processing in golden retriever muscular dystrophy, an animal homologue of Duchenne muscular dystrophy. Genomics 13: 115–121.
8. Béroud C, Tuffery-Giraud S, Matsuo M, Hamroun D, Humbertclaude V, et al. (2007) Multiexon skipping leading to an artificial DMD protein lacking amino acids from exons 45 through 55 could rescue up to 63% of patients with Duchenne muscular dystrophy. Hum Mutat 28: 196–202.
9. Wee K, Pramono Z, Wang J, MacDorman K, Lai P, et al. (2008) Dynamics of co-transcriptional pre-mRNA folding influences the induction of dystrophin exon skipping by antisense oligonucleotides. PLoS ONE 3: e1844.
10. Pramono Z, Takeshima Y, Alimsardjono H, Ishii A, Takeda S, et al. (1996) Induction of exon skipping of the dystrophin transcript in lymphoblastoid cells by transfecting an antisense oligodeoxynucleotide complementary to an exon recognition sequence. Biochem Biophys Res Commun 226: 445–449.
11. Chelly J, Gilgenkrantz H, Hugnot J, Hamard G, Lambert M, et al. (1991) Illegitimate transcription. Application to the analysis of truncated transcripts of the dystrophin gene in nonmuscle cultured cells from Duchenne and Becker patients. J Clin Invest 88: 1161–1166.
12. Aartsma-Rus A, Janson A, Kaman W, Bremmer-Bout M, den Dunnen J, et al. (2003) Therapeutic antisense-induced exon skipping in cultured muscle cells from six different DMD patients. Hum Mol Genet 12: 907–914.
13. Aartsma-Rus A, Janson A, Kaman W, Bremmer-Bout M, van Ommen G, et al. (2004) Antisense-induced multiexon skipping for Duchenne muscular dystrophy makes more sense. Am J Hum Genet 74: 83–92.
14. Gonçalves M, Swildens J, Holkers M, Narain A, van Nierop G, et al. (2008) Genetic complementation of human muscle cells via directed stem cell fusion. Mol Ther 16: 741–748.
15. Cooper S, Kizana E, Yates J, Lo H, Yang N, et al. (2007) Dystrophinopathy carrier determination and detection of protein deficiencies in muscular dystrophy using lentiviral MyoD-forced myogenesis. Neuromuscul Disord 17: 276–284.
16. Zheng J, Wang Y, Karandikar A, Wang Q, Gai H, et al. (2006) Skeletal myogenesis by human embryonic stem cells. Cell Res 16: 713–722.
17. McClorey G, Moulton H, Iversen P, Fletcher S, Wilton S (2006) Antisense oligonucleotide-induced exon skipping restores dystrophin expression in vitro in a canine model of DMD. Gene Ther 13: 1373–1381.
18. Reiss J, Rininsland F (1994) An explanation for the constitutive exon 9 cassette splicing of the DMD gene. Hum Mol Genet 3: 295–298.
19. Miller A, Buttimore C (1986) Redesign of retrovirus packaging cell lines to avoid recombination leading to helper virus production. Mol Cell Biol 6: 2895–2902.
20. Morgenstern J, Land H (1990) A series of mammalian expression vectors and characterisation of their expression of a reporter gene in stably and transiently transfected cells. Nucleic Acids Res 18: 1068.
21. Choi J, Costa M, Mermelstein C, Chagas C, Holtzer S, et al. (1990) MyoD converts primary dermal fibroblasts, chondroblasts, smooth muscle, and retinal pigmented epithelial cells into striated mononucleated myoblasts and multinucleated myotubes. Proc Natl Acad Sci U S A 87: 7988–7992.
22. Etzion S, Barbash I, Feinberg M, Zarin P, Miller L, et al. (2002) Cellular cardiomyoplasty of cardiac fibroblasts by adenoviral delivery of MyoD ex vivo: an unlimited source of cells for myocardial repair. Circulation 106: I125–130.
23. Noda T, Fujino T, Mie M, Kobatake E (2009) Transduction of MyoD protein into myoblasts induces myogenic differentiation without addition of protein transduction domain. Biochem Biophys Res Commun 382: 473–477.
24. Shimatsu Y, Yoshimura M, Yuasa K, Urasawa N, Tomohiro M, et al. (2005) Major clinical and histopathological characteristics of canine X-linked muscular dystrophy in Japan, CXMDJ. Acta Myol 24: 145–154.
25. Mitrpant C, Adams A, Meloni P, Muntoni F, Fletcher S, et al. (2009) Rational design of antisense oligomers to induce dystrophin exon skipping. Mol Ther 17: 1418–1426.
26. Aartsma-Rus A, Kaman W, Weij R, den Dunnen J, van Ommen G, et al. (2006) Exploring the frontiers of therapeutic exon skipping for Duchenne muscular dystrophy by double targeting within one or multiple exons. Mol Ther 14: 401–407.
27. Harding P, Fall A, Honeyman K, Fletcher S, Wilton S (2007) The influence of antisense oligonucleotide length on dystrophin exon skipping. Mol Ther 15: 157–166.
28. Aartsma-Rus A, van Ommen G (2007) Antisense-mediated exon skipping: a versatile tool with therapeutic and research applications. RNA 13: 1609–1624.
29. Wilton S, Fall A, Harding P, McClorey G, Coleman C, et al. (2007) Antisense oligonucleotide-induced exon skipping across the human dystrophin gene transcript. Mol Ther 15: 1288–1296.
30. McClorey G, Fall A, Moulton H, Iversen P, Rasko J, et al. (2006) Induced dystrophin exon skipping in human muscle explants. Neuromuscul Disord 16: 583–590.
31. Aartsma-Rus A, De Winter C, Janson A, Kaman W, Van Ommen G, et al. (2005) Functional analysis of 114 exon-internal AONs for targeted DMD exon skipping: indication for steric hindrance of SR protein binding sites. Oligonucleotides 15: 284–297.
32. Hallegger M, Llorian M, Smith C (2010) Alternative splicing: global insights. FEBS J 277: 856–866.
33. Sironi M, Cagliani R, Pozzoli U, Bardoni A, Comi G, et al. (2002) The dystrophin gene is alternatively spliced throughout its coding sequence. FEBS Lett 517: 163–166.
34. Pruitt K, Harrow J, Harte R, Wallin C, Diekhans M, et al. (2009) The consensus coding sequence (CCDS) project: Identifying a common protein-coding gene set for the human and mouse genomes. Genome Res 19: 1316–1323.
35. Desmet F, Hamroun D, Lalande M, Collod-Béroud G, Claustres M, et al. (2009) Human Splicing Finder: an online bioinformatics tool to predict splicing signals. Nucleic Acids Res 37: e67.

Efficient gene transfer into neurons in monkey brain by adeno-associated virus 8

Yoshito Masamizu[a], Takashi Okada[b], Hidetoshi Ishibashi[a], Shin'ichi Takeda[b], Shigeki Yuasa[c] and Kiyoshi Nakahara[a,d]

Although the adeno-associated virus (AAV) vector is a promising tool for gene transfer into neurons, especially for therapeutic purposes, neurotropism in primate brains is not fully elucidated for specific AAV serotypes. Here, we injected AAV serotype 8 (AAV8) vector carrying the enhanced green fluorescent protein (EGFP) gene under a ubiquitous promoter into the cerebral cortex, striatum and substantia nigra of common marmosets. Robust neuronal EGFP expression was observed at all injected sites. Cell typing with immunohistochemistry confirmed efficient AAV8-mediated gene transfer into the pyramidal neurons in the cortex, calbindin-positive medium spiny neurons in the striatum and dopaminergic neurons in the substantia nigra. The results indicate a preferential tropism of AAV8 for subsets of neurons, but not for glia, in monkey brains. *NeuroReport* **21:447–451 © 2010 Wolters Kluwer Health | Lippincott Williams & Wilkins.**

NeuroReport 2010, 21:447–451

Keywords: adeno-associated virus, gene transfer, marmoset, motor cortex, neuron, nonhuman primate, striatum, substantia nigra, tropism

[a]Department of Animal Models for Human Disease, [b]Department of Molecular Therapy, [c]Department of Ultrastructural Research, National Institute of Neuroscience, NCNP and [d]PRESTO, Japan Science and Technology Agency

Correspondence to Dr Kiyoshi Nakahara, Department of Animal Models for Human Disease, National Institute of Neuroscience, NCNP, 4-1-1 Ogawa-Higashi, Kodaira, Tokyo 187-8502, Japan
Tel: +81 42 346 1724; fax: +81 42 346 1754; e-mail: nakahara@ncnp.go.jp

Received 24 January 2010 accepted 14 February 2010

Introduction

Adeno-associated virus (AAV) vectors are promising as a means to deliver genes into a wide range of tissues *in vivo*. They are eligible as gene therapy vectors, as qualified by their nonpathogenicity and long-term gene expression, and are particularly suitable for gene transfer into neurons of the central nervous system (CNS) because of their ability to infect nondividing cells [1,2]. In addition to their therapeutic applications, AAV-mediated gene transfer into the CNS is becoming increasingly valuable in basic neurophysiological research, particularly with the advent of genetic methods for experimental manipulation of neuronal activities, such as optogenetics [3,4]. Extensive exploration of the neurotropism of AAV vectors in primate brains is thus prerequisite for application to the gene therapy of neurological disorders and to neurophysiological research.

One remarkable feature of AAV vectors is their wide variety of serotypes originating from the variation in the amino acid sequence of the capsid proteins. Infection efficiency and cell tropism of the AAV vectors are mainly determined by their serotypes, which can directly affect epitopes recognized by the host immune system and preference for the receptors used for cell entry [1]. This feature also offers researchers opportunities for selecting an appropriate AAV serotype according to their purposes and target cells. Although AAV serotype 2 (AAV2) has been the most commonly used in both clinical applications and basic research among at least 100 identified serotypes [1], recent studies have revealed the potential and advantages of other serotypes [1,5–8]. Among these, adeno-associated virus serotype 8 (AAV8) has attracted interest for its higher efficiency than AAV2 in transferring genes into CNS neurons [9]. However, neuronal tropism of AAV8 has mainly been investigated in rodent brains, and tropism of AAV8 for neuronal cell types in primate brains is not yet fully elucidated.

Here, we investigated tropism and gene transfer efficiency of AAV8 vector in the brain of a new world monkey, the common marmoset. More specifically, we explored the ability of AAV8 to deliver genes into projection neurons in the striatum and dopaminergic neurons in the substantia nigra. These neurons constitute functional circuits within the extrapyramidal system, playing pivotal roles not only in normal functions such as action selection, but also in the pathophysiology of various neurological disorders such as Parkinson's disease [10–13]. This study reveals strong neuronal tropism of AAV8, as identified by several markers for neuronal subtypes in the pyramidal and extrapyramidal systems of the primate brain.

Methods

Monkeys

Two laboratory-bred adult male common marmosets (*Callithrix jacchus*) were used. The animals were 59 months (weight, 325 g) and 62 months (weight, 358 g) of age at the start of the experiment. Animal experiments were conducted in accordance with the NIH guidelines for the care and use of laboratory animals, and with the guidelines approved by the ethics committee for primate research of the National Center of Neurology and Psychiatry, Japan.

0959-4965 © 2010 Wolters Kluwer Health | Lippincott Williams & Wilkins

DOI: 10.1097/WNR.0b013e328338ba00

Virus preparation

AAV8-enhanced green fluorescent protein (EGFP) virus production and purification was performed as described earlier [14,15]. The vector plasmid (pAAV-EGFP) contained EGFP cDNA and the woodchuck hepatitis virus post-transcriptional regulatory element (WPRE) under the control of the CAG promoter, a modified chicken β-actin promoter with a cytomegalovirus immediate early enhancer. The pAAV-EGFP vector was cotransfected with an AAV8 chimeric helper plasmid encoding the AAV2 rep gene and the AAV8 cap gene, and an adenoviral helper plasmid pAdeno [16], into HEK293 cells by calcium phosphate coprecipitation with the use of active gassing [15]. Cell suspensions were collected 72 h after transfection, and centrifuged at 300 × *g* for 10 min. Cell pellets were resuspended in 30 ml of Tris-buffered saline [100 mM Tris–HCl (pH 8.0), 150 mM NaCl]. AAV8-EGFP virus was harvested by five cycles of freeze-thawing of the resuspended pellet. The crude viral lysate was initially concentrated by a brief two-tier CsCl gradient centrifugation for 3 h [17], and further purified by dual ion-exchange chromatography [14]. The final number of AAV8-EGFP virus particles was determined by quantitative polymerase chain reaction of DNase I-treated stocks with plasmid standards, and was 3.0×10^{13} vector genomes (vg)/ml.

Virus injections

All surgical procedures and AAV8-EGFP virus injections were performed under aseptic conditions. Animals were initially anesthetized with 0.1 ml ketamine (50 mg/ml, intramuscularly). Animals were then intubated and placed in a stereotaxic apparatus with anesthesia maintained using inhaled isoflurane (1.5–2.5% in oxygen). Pulse oxygen (SpO_2), heart rate, body temperature, end-tidal CO_2 ($EtCO_2$), O_2 (EtO_2), isoflurane (EtISO), and fraction of inspired CO_2 ($FiCO_2$), O_2 (FiO_2), and isoflurane (FiISO) were continuously monitored to judge the animal's condition. After injection of 0.07 ml cefovecin (80 mg/ml, intramuscularly) as an antibiotic, a stereotaxic small craniotomy (2–3 mm in diameter) was then made over the area of interest, and the underlying dura was slit to allow penetration by the virus-containing 10-μl Hamilton syringe connected to a 33 G (45°angle) needle. Virus solution (3 μl) was injected at a rate of 0.25 μl/min to each site. Injection sites were determined using the Stereotaxic Atlas of the Marmoset Brain with Immunohistochemical Architecture and MRI Images (by Yuasa S, Nakamura K and Kohsaka S, in press). As injection sites, we aimed at the primary motor cortex: anterior (A) 12.0 mm from the interaural line, lateral (L) 6.8 mm from the midline, and ventral (V) 2.5 mm from the brain surface [18], the striatum: A 12.0 mm, L 3.0 mm, and V 6.0 mm [19], and the substantia nigra: A 5.5 mm, L 2.5 mm, and V 11.7 mm [20]. After each injection, the needle was kept in place for an additional 15 min (motor cortex) or 5 min (striatum and substantia nigra), and then slowly withdrawn (2 mm/min). We then waited 4 weeks after the virus injection for EGFP expression to appear.

Immunohistochemistry

The procedures were as reported earlier [21], with slight modifications. Briefly, 4 weeks after AAV8-EGFP virus injection, the animals were deeply anesthetized by an intraperitoneal injection of sodium pentobarbital, and then perfused through the ascending aorta with 4% paraformaldehyde dissolved in 0.1 M phosphate-buffered saline (PBS, pH 7.4). The brains were sampled, and then postfixed at 4°C for 3 days with the same fixative. The fixed brains were embedded in 3% agar in PBS, and then sliced coronally into 100 μm sections with a Microslicer (DTK-3000, DOSAKA EM, Kyoto, Japan). Immunohistochemical stainings were performed on free-floating sections. After 1 h of preincubation with 10% normal goat serum at 4°C, sections were incubated with primary antibodies in PBS containing 2% Triton X-100 at 4°C overnight. Antibodies against the following neuronal or glial marker proteins were used: neuron-specific nuclear protein (NeuN; mouse IgG, 1 : 500; Cat. No. MAB377, Millipore, Billerica, Massachusetts, USA), nonphosphorylated neurofilament protein (NNF; mouse IgG, 1 : 1000; Cat. No. SMI-32R, Sternberger Monoclonals, Baltimore, Maryland, USA) [22], calbindin D-28k (rabbit IgG, 1 : 1000; Cat. No. CB38a, Swant, Bellinzona, Switzerland), tyrosine hydroxylase (TH; mouse IgG, 1 : 1000; Cat. No. T2928, Sigma-Aldrich, St. Louis, Missouri, USA), glial fibrillary acidic protein (GFAP; rabbit IgG, 1 : 200; Cat. No. Z0334, Dako, Glostrup, Denmark), and oligodendrocyte transcription factor 2 (Olig2; rabbit IgG, 1 : 2000; Cat. No. AB9610, Millipore). Sections were then rinsed eight times with PBS, and incubated with secondary antibodies in PBS at 4°C for 5 h. Appropriate secondary antibody [Alexa goat anti-mouse 594 IgG (1 : 500; Cat. No. A11005, Molecular Probes, Eugene, Oregon, USA), or Alexa goat anti-rabbit 594 IgG (1 : 500; Cat. No. A11012, Molecular Probes)] directed against the species in which the primary antibody was raised, was used in each case. Sections were then rinsed five times with PBS. The stained sections were mounted on glass slides with Fluoromount-G (Beckman Coulter, Fullerton, California, USA) and examined with a confocal laser-scanning microscope (LSM5 Pascal, Zeiss, Oberkochen, Germany). EGFP expression was directly observed through confocal fluorescence images.

Results

Neuronal tropism of AAV8 in the marmoset brain *in vivo*

We injected recombinant AAV8 vector carrying the EGFP gene under the control of CAG promoter (AAV8-EGFP) into the brains of two common marmosets. Stereotaxic virus injections were carried out aiming at the motor cortex, the striatum and the substantia nigra. Four weeks after the injections, intense EGFP fluorescence was

directly observed in numerous cell bodies and fibers around all injected sites, indicating efficient EGFP gene transfer by the infection of AAV8-EGFP (Figs 1 and 2). As the CAG promoter has strong and ubiquitous activity, the types of EGFP-expressing ($EGFP^+$) cells would reflect endogenous tropism of AAV8 in the primate brain. Thus, we examined the tropism of AAV8-EGFP by immunostaining for neuronal or glial marker proteins. Confocal microscopic observations revealed that almost all of the $EGFP^+$ cells in the striatum were colocalized with NeuN (Fig. 1a–c). In contrast, the $EGFP^+$ cells were rarely colocalized with GFAP, or with Olig2, marker proteins for astrocytes and oligodendrocytes, respectively (Fig. 1d–i). These results indicated tropism of AAV8 for neurons, but not for glia, in the primate brain.

Identification of AAV8-infected neuronal cell types

We further characterized the $EGFP^+$ neurons by immunostaining for several markers of neuronal subtypes. In the motor cortex, most of the $EGFP^+$ cells were pyramidal neurons, as revealed by the coexpression of NNF, a cytoskeletal protein found in a subset of pyramidal neurons (Fig. 2a–d). Overlaps of EGFP fluorescence and NNF expression were evident in the apical dendrites (Fig. 2d). In the striatum, the $EGFP^+$ cells exhibited morphology characteristic of medium spiny neurons, the principal cell type in this region. Indeed, immunostaining confirmed that the majority of the $EGFP^+$ cells coexpressed calbindin, a specific marker for the medium spiny neuron [23] (Fig. 2e–h). We also found colocalization of EGFP fluorescence and TH immunoreactivity, a specific marker for dopaminergic neurons, in the substantia nigra (Fig. 2i–l).

Quantification of AAV8 infection efficiency in the identified neuronal cell types

Finally, to quantify the neuronal tropism of AAV8, we counted colocalizations of EGFP fluorescence and immunohistochemical staining of neuronal or glial marker proteins in the three injected regions ($n = 2$, Table 1). The majority of the $EGFP^+$ cells were colocalized with neuronal marker proteins, and the estimated percentages of colocalization were extremely high: 91% of the $EGFP^+$ cells colocalized with NNF in the motor cortex, 70% with calbindin in the striatum, and 99% with TH in the substantia nigra pars compacta. In the striatum, we also counted colocalizations of EGFP signal with NeuN, and the estimated percentage of colocalization reached 98%. In contrast, we hardly detected colocalization of the $EGFP^+$ cells with GFAP or with Olig2 in the three brain regions examined (3% or below).

Discussion

In this study, we injected AAV8-EGFP into three brain regions, the motor cortex, the striatum and the substantia nigra of two common marmosets. Almost all of the

Fig. 1

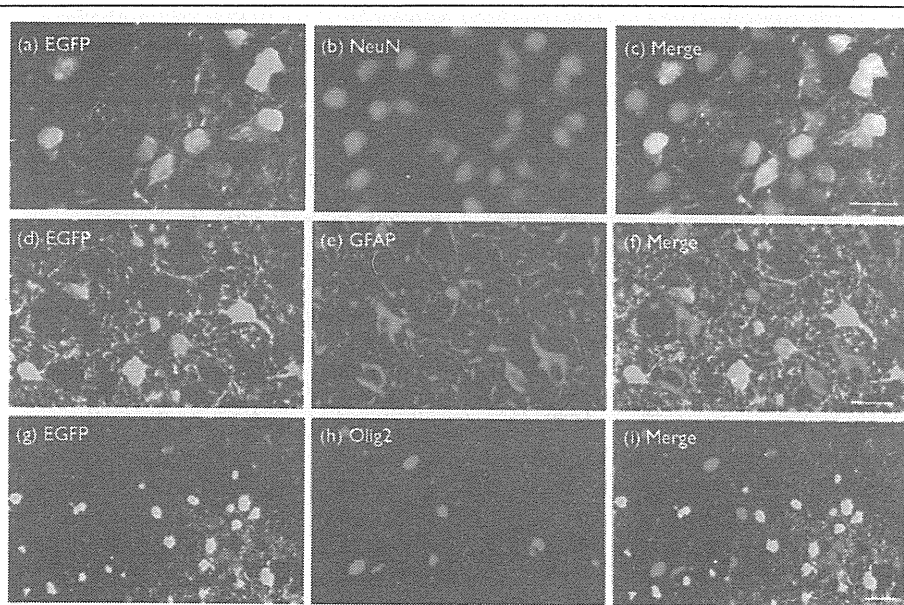

Adeno-associated virus serotype 8 preferentially transfers the enhanced green fluorescent protein (EGFP) gene into neurons in the primate striatum *in vivo*. Confocal images show EGFP-positive ($EGFP^+$) cells in the striatum (a, d, g; green). $EGFP^+$ cells are colocalized with neuron-specific nuclear protein (NeuN, b; red) as shown by the merged image (c; yellow). $EGFP^+$ cells are rarely colocalized with glial fibrillary acidic protein (GFAP, e; red) or oligodendrocyte transcription factor 2 (Olig2, h; red) as shown by the merged images (f and i). Bars: 20 μm.

Fig. 2

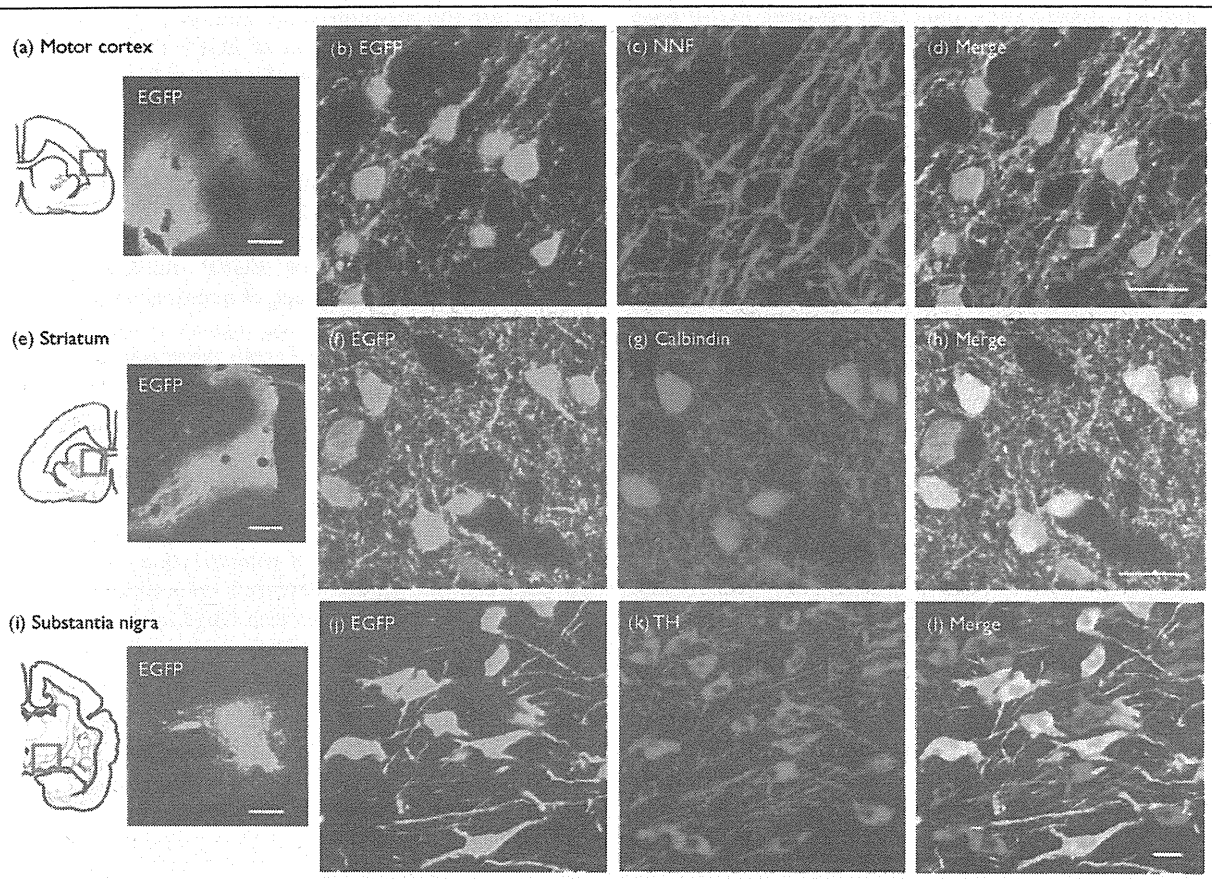

Identification of cell types of adeno-associated virus 8-infected neurons in the motor cortex, the striatum and the substantia nigra. Confocal images with a low-power field show native enhanced green fluorescent protein (EGFP) fluorescence at the three injection sites (a, e, i; green), approximately corresponding to the red boxes on the insets of coronal marmoset brain maps. High-power confocal images show $EGFP^+$ cells (green) in the motor cortex (b), the striatum (f) and the substantia nigra (j). $EGFP^+$ cells are colocalized with non-phosphorylated neurofilament protein (NNF, c; red), calbindin (g; red), and tyrosine hydroxylase (TH, k; red) as shown by the merged images (d, h, l; yellow). Bars represent 500 μm in (a), (e), (i), and 20 μm in (d), (h), (l).

Table 1 Quantification of infection efficiency in identified neuronal cell types after AAV8-EGFP virus injection

Injection site	Neuron (neuronal marker$^+$/ $EGFP^+$cells)	Astrocyte ($GFAP^+$/ $EGFP^+$cells)	Oligodendrocyte ($Olig2^+$/ $EGFP^+$cells)
Motor cortex	91% (169/185)	1% (2/189)	0% (0/197)
Striatum	98% (190/193)a 70% (142/202)b	0% (0/195)	1% (2/207)
Substantia nigra pars compacta	99% (190/192)	0% (0/193)	3% (5/190)

NNF in the motor cortex, NeuN (a) and calbindin (b) in the striatum, and TH in the substantia nigra were used as the neuronal marker.
AAV, adeno-associated virus; EGFP, enhanced green fluorescence protein; GFAP, glial fibrillary acidic protein; NeuN, neuron-specific nuclear protein; NNF, nonphosphorylated neurofilament protein; Olig2, oligodendrocyte transcription factor 2; TH, tyrosine hydroxylase.

$EGFP^+$ cells in each injected site were colocalized with neuron-specific markers. In contrast, we rarely found colocalization of EGFP fluorescence with specific marker proteins for glial cells. As we used a ubiquitous promoter (CAG promoter) in this study, the present results indicate endogenous AAV8 tropism for neurons, but not for glia, in marmoset brains *in vivo*. The neuronal tropism of AAV8 revealed in the present study is consistent with an earlier study in cynomolgus monkeys [24]. It has been shown that AAV8 could transfect astroglia in primary culture prepared from newborn rats, but rarely *in vivo* in rat hippocampus [25]. Therefore, the degree of neurotropism of AAV8 may depend on the infection conditions (*in vivo* vs. *in vitro*).

In the present study, we examined EGFP expression 4 weeks after injection of AAV8-EGFP. Eslamboli *et al.* [20] showed long-term (at least 1 year) transgene expression through AAV5 in the marmoset substantia nigra. Thus, it is likely that AAV8 also enables stable transgene expression in primate brains for long periods.

One main goal of this study was to examine the ability of AAV8 to transfer foreign genes into identified neuronal cell types in primate brain. Specifically, we explored the ability of AAV8 to transfect projection neurons in the striatum and dopaminergic neurons in the substantia nigra, which constitute functional circuits within the nigrostriatal loop [10–13]. Clinically, dysfunctions of the basal ganglia circuit have been related to many neurological disorders including Parkinson's disease and Huntington's disease. AAV-mediated gene transfer is one of the most promising means for gene therapy of these diseases, and preclinical investigations of the tropism of AAV for functionally identified neurons are requisite steps for future practical applications. In this study, we successfully showed efficient AAV8 transfection of calbindin-positive neurons in the striatum and TH-positive dopaminergic neurons in the substantia nigra. These results indicate the potential of AAV8 vector as a therapeutic tool for basal ganglia-related diseases. Other than the therapeutic applications, AAV8 will be useful to deliver molecular tools to experimentally monitor or manipulate neuronal activities in primate brains [3,4]. Further research is needed to clarify the infection spectrum of AAV8 and other AAV serotypes in many other neuronal cell types in the primate brain.

Conclusion

AAV8 vector has strong tropism for neurons but not for glia in the brain of the common marmoset *in vivo*. Efficient AAV8-mediated gene transfer into identified neuronal cell types, calbindin-positive medium spiny neurons in the striatum and TH-positive dopaminergic neurons in the substantia nigra, was also successfully shown.

Acknowledgements

This work was supported by a JSPS Research Fellowship for Young Scientists (Y.M.), and by PRESTO, JST (K.N.). All the authors declare that they have no conflict of interest.

References

1 Daya S, Berns KI. Gene therapy using adeno-associated virus vectors. *Clin Microbiol Rev* 2008; **21**:583–593.
2 Kaplitt MG, Leone P, Samulski RJ, Xiao X, Pfaff DW, O'Malley KL, *et al.* Long-term gene expression and phenotypic correction using adeno-associated virus vectors in the mammalian brain. *Nat Genet* 1994; **8**:148–154.
3 Zhang F, Aravanis AM, Adamantidis A, de Lecea L, Deisseroth K. Circuit-breakers: optical technologies for probing neural signals and systems. *Nat Rev Neurosci* 2007; **8**:577–581.
4 Han X, Qian X, Bernstein JG, Zhou HH, Franzesi GT, Stern P, *et al.* Millisecond-timescale optical control of neural dynamics in the nonhuman primate brain. *Neuron* 2009; **62**:191–198.
5 Ohshima S, Shin JH, Yuasa K, Nishiyama A, Kira J, Okada T, *et al.* Transduction efficiency and immune response associated with the administration of AAV8 vector into dog skeletal muscle. *Mol Ther* 2009; **17**:73–80.
6 Zincarelli C, Soltys S, Rengo G, Rabinowitz JE. Analysis of AAV serotypes 1-9 mediated gene expression and tropism in mice after systemic injection. *Mol Ther* 2008; **16**:1073–1080.
7 Gao GP, Alvira MR, Wang L, Calcedo R, Johnston J, Wilson JM. Novel adeno-associated viruses from rhesus monkeys as vectors for human gene therapy. *Proc Natl Acad Sci U S A* 2002; **99**:11854–11859.
8 Rutledge EA, Halbert CL, Russell DW. Infectious clones and vectors derived from adeno-associated virus (AAV) serotypes other than AAV type 2. *J Virol* 1998; **72**:309–319.
9 Broekman ML, Comer LA, Hyman BT, Sena-Esteves M. Adeno-associated virus vectors serotyped with AAV8 capsid are more efficient than AAV-1 or -2 serotypes for widespread gene delivery to the neonatal mouse brain. *Neuroscience* 2006; **138**:501–510.
10 Nicola SM, Surmeier J, Malenka RC. Dopaminergic modulation of neuronal excitability in the striatum and nucleus accumbens. *Annu Rev Neurosci* 2000; **23**:185–215.
11 Nambu A, Tokuno H, Takada M. Functional significance of the cortico-subthalamo-pallidal, hyperdirect, pathway. *Neurosci Res* 2002; **43**:111–117.
12 Redgrave P, Gurney K. The short-latency dopamine signal: a role in discovering novel actions? *Nat Rev Neurosci* 2006; **7**:967–975.
13 Obeso JA, Marin C, Rodriguez-Oroz C, Blesa J, Benitez-Temino B, Mena-Segovia J, *et al.* The basal ganglia in Parkinson's disease: current concepts and unexplained observations. *Ann Neurol* 2008; **64 (Suppl 2)**:S30–S46.
14 Okada T, Nonaka-Sarukawa M, Uchibori R, Kinoshita K, Hayashita-Kinoh H, Nitahara-Kasahara Y, *et al.* Scalable purification of adeno-associated virus serotype 1 (AAV1) and AAV8 vectors, using dual ion-exchange adsorptive membranes. *Hum Gene Ther* 2009; **20**:1013–1021.
15 Okada T, Nomoto T, Yoshioka T, Nonaka-Sarukawa M, Ito T, Ogura T, *et al.* Large-scale production of recombinant viruses by use of a large culture vessel with active gassing. *Hum Gene Ther* 2005; **16**:1212–1218.
16 Matsushita T, Elliger S, Elliger C, Podsakoff G, Villarreal L, Kurtzman GJ, *et al.* Adeno-associated virus vectors can be efficiently produced without helper virus. *Gene Ther* 1998; **5**:938–945.
17 Okada T, Shimazaki K, Nomoto T, Matsushita T, Mizukami H, Urabe M, *et al.* Adeno-associated viral vector-mediated gene therapy of ischemia-induced neuronal death. *Methods Enzymol* 2002; **346**:378–393.
18 Burman KJ, Palmer SM, Gamberini M, Spitzer MW, Rosa MG. Anatomical and physiological definition of the motor cortex of the marmoset monkey. *J Comp Neurol* 2008; **506**:860–876.
19 Eslamboli A, Georgievska B, Ridley RM, Baker HF, Muzyczka N, Burger C, *et al.* Continuous low-level glial cell line-derived neurotrophic factor delivery using recombinant adeno-associated viral vectors provides neuroprotection and induces behavioral recovery in a primate model of Parkinson's disease. *J Neurosci* 2005; **25**:769–777.
20 Eslamboli A, Romero-Ramos M, Burger C, Bjorklund T, Muzyczka N, Mandel RJ, *et al.* Long-term consequences of human alpha-synuclein overexpression in the primate ventral midbrain. *Brain* 2007; **130**:799–815.
21 Nakahira E, Yuasa S. Neuronal generation, migration, and differentiation in the mouse hippocampal primordium as revealed by enhanced green fluorescent protein gene transfer by means of in utero electroporation. *J Comp Neurol* 2005; **483**:329–340.
22 Bourne JA, Warner CE, Rosa MG. Topographic and laminar maturation of striate cortex in early postnatal marmoset monkeys, as revealed by neurofilament immunohistochemistry. *Cereb Cortex* 2005; **15**:740–748.
23 Parent A, Fortin M, Cote PY, Cicchetti F. Calcium-binding proteins in primate basal ganglia. *Neurosci Res* 1996; **25**:309–334.
24 Dodiya HB, Bjorklund T, Stansell Iii J, Mandel RJ, Kirik D, Kordower JH. Differential transduction following basal ganglia administration of distinct pseudotyped AAV capsid serotypes in nonhuman primates. *Mol Ther* 2009; doi:10.1038/mt.2009.216.
25 Klein RL, Dayton RD, Leidenheimer NJ, Jansen K, Golde TE, Zweig RM. Efficient neuronal gene transfer with AAV8 leads to neurotoxic levels of tau or green fluorescent proteins. *Mol Ther* 2006; **13**:517–527.

EXPERIMENTAL CELL RESEARCH 316 (2010) 2932–2944

available at www.sciencedirect.com

ScienceDirect

www.elsevier.com/locate/yexcr

Research Article

Six family genes control the proliferation and differentiation of muscle satellite cells

Hiroshi Yajima[a], *Norio Motohashi*[b], *Yusuke Ono*[b], *Shigeru Sato*[a], *Keiko Ikeda*[a], *Satoru Masuda*[b], *Erica Yada*[b], *Hironori Kanesaki*[b], *Yuko Miyagoe-Suzuki*[b], *Shin'ichi Takeda*[b], *Kiyoshi Kawakami*[a,*]

[a]*Division of Biology, Center for Molecular Medicine, Jichi Medical University, Tochigi, Japan*
[b]*Department of Molecular Therapy, National Institute of Neuroscience, National Center of Neurology and Psychiatry, Tokyo, Japan*

ARTICLE INFORMATION

Article Chronology:
Received 1 April 2010
Revised version received 19 July 2010
Accepted 3 August 2010
Available online 6 August 2010

Keywords:
Muscle satellite cell
Six gene
Cell proliferation
Muscle differentiation
Retrovirus-mediated overexpression
Gene knockdown

ABSTRACT

Muscle satellite cells are essential for muscle growth and regeneration and their morphology, behavior and gene expression have been extensively studied. However, the mechanisms involved in their proliferation and differentiation remain elusive. Six1 and Six4 proteins were expressed in the nuclei of myofibers of adult mice and the numbers of myoblasts positive for Six1 and Six4 increased during regeneration of skeletal muscles. Six1 and Six4 were expressed in quiescent, activated and differentiated muscle satellite cells isolated from adult skeletal muscle. Overexpression of *Six4* and *Six5* repressed the proliferation and differentiation of satellite cells. Conversely, knockdown of Six5 resulted in augmented proliferation, and that of Six4 inhibited differentiation. Muscle satellite cells isolated from *Six4*$^{+/-}$*Six5*$^{-/-}$ mice proliferated to higher cell density though their differentiation was not altered. Meanwhile, overproduction of Six1 repressed proliferation and promoted differentiation of satellite cells. In addition, Six4 and Six5 repressed, while Six1 activated *myogenin* expression, suggesting that the differential regulation of *myogenin* expression is responsible for the differential effects of *Six* genes. The results indicated the involvement of *Six* genes in the behavior of satellite cells and identified *Six* genes as potential target for manipulation of proliferation and differentiation of muscle satellite cells for therapeutic applications.

Introduction

Muscle satellite cells are tissue-specific stem cells that reside beneath the basal lamina surrounding the myofibers of mature adult skeletal muscles and play a major role in post-natal muscle growth and regeneration [1, for review see 2]. In the intact adult muscles, satellite cells are mitotically quiescent, while in the injured or damaged muscle, they are activated to proliferate, differentiate and then regenerate myofibers by fusing with each other or with residual fibers. The recent discovery of specific markers for muscle satellite cells, including Pax7, M-cadherin, MyoD and myogenin, has allowed the identification of the status of these cells [2]. Pax7 and M-cadherin is expressed in quiescent satellite cells, while MyoD is rapidly induced during activation of satellite cells [3]. The Pax7- and MyoD-double-positive cells are regarded as transit amplifying cells and future myoblasts [3]. It is

* *Corresponding author.* Division of Biology, Center for Molecular Medicine, Jichi Medical University, 3311-1, Yakushiji, Shimotsuke, Tochigi, 329-0498, Japan. Fax: +81 285 44 5476.
E-mail address: kkawakam@jichi.ac.jp (K. Kawakami).

0014-4827/$ – see front matter © 2010 Elsevier Inc. All rights reserved.
doi:10.1016/j.yexcr.2010.08.001

noted that some transit amplifying cells become MyoD-negative, and those are thought to re-enter the quiescent state [3]. The expression of Pax7 is down-regulated before commitment to terminal differentiation. Despite such progress in our understanding of the lineage and behavior of muscle satellite cells, there are other areas that remain poorly understood; for example, the exact mechanism that orchestrates the proliferation and differentiation of these cells.

Recently, we developed a new and efficient method to isolate quiescent satellite cells using monoclonal antibody SM/C-2.6 [4]. SM/C-2.6-positive cells co-express M-cadherin and become MyoD-positive in growth media. They are differentiated into desmin- and MyoD-positive myofibers under differentiation conditions. In the same study, we showed that the sorted muscle satellite cells differentiated into muscle fibers following their injection into *mdx* mouse muscles [4]. Furthermore, genome-wide gene expression analysis using the isolated cells allowed the identification of a quiescent cell-specific marker, calcitonin receptor (CTR), implicating the involvement of calcitonin/CTR signaling in the activation of satellite cells [5]. Thus, the SM/C-2.6-positive satellite cells are useful tool for investigating the mechanism of regulation of proliferation and differentiation *in vitro* and allow us to gain a better understanding of the role of satellite cells during muscle regeneration, compared to the use of cell lines such as C2C12 and MM14 cells.

The *Six* genes have been identified as homologues of *Drosophila sine oculis*, which is crucial for compound-eye formation [6,7]. The mammalian *Six* gene family consists of six members, *Six1* to *Six6* [8]. During development, *Six1* and *Six4* play important roles in the formation of various organs, such as olfactory epithelium, cranial ganglia, inner ear, kidney, skeletal muscle and skeleton [9–20]. During skeletal muscle development, *Six1* and *Six4* are expressed in the somite and migrating myoblasts and play important roles in myogenesis [21–23]. Another member of the *Six* gene family, *Six5*, is expressed in the somite and adult skeletal muscles [22,24,25]. Genetic ablation of both *Six1* and *Six4* results in gross muscle hypoplasia [21]. Limb muscles derived from hypaxial progenitors disappear, as a result of aberrant migration and apoptosis of myoblasts, which are caused by down-regulation of Pax3. Epaxial and other hypaxial muscles are impaired through severely compromised expression of myogenic regulatory factors (MRF) genes, Mrf4 and myogenin, within the myotome [21]. Expression of myogenin is thought to be directly controlled by Six1, Six4 and Six5 via MEF3 sites *in vivo* [26] and in cultured cells [27]. Moreover, *Six1* and *Six4* are necessary for the induction of the fast-type-muscle program during myogenesis [23] and are involved in the assignment of the fast/glycolytic character of the myofiber in adult skeletal muscles [22]. However, there is virtually no information on the role of *Six1*, *Six4* and *Six5* in muscle regeneration, especially in the proliferation and differentiation of muscle satellite cells.

In the present study, we analyzed the expression of *Six1*, *Six4* and *Six5* in adult skeletal muscles during regeneration and in satellite cells *in vivo* and in culture. We examined the effects of overexpression and knockdown of *Six* genes on the proliferation and differentiation of isolated satellite cells *in vitro*. Finally, the proliferation and differentiation of muscle satellite cells isolated from *Six4*- and *Six5*-deficient mice were compared to those of wild-type mice. The results demonstrated the involvement of *Six* genes in the regulation of proliferation and differentiation of muscle satellite cells.

Results

Induction of expression of Six proteins during regeneration of adult skeletal muscle

To investigate the expression of *Six* genes during skeletal muscle regeneration, we induced muscle damage by injecting cardiotoxin into the tibialis anterior (TA) muscles of 8- to 12-week-old wild-type mice. Three days after the injection, transverse sections of TA muscles were prepared from the injected as well as intact mice and mapped the distribution of Six proteins by immunofluorescence using specific antibodies to Six1 and Six4 [10,18]. In the intact non-injected TA muscles, a considerable number of muscle nuclei was positive for Six1 (Fig. 1A). The Six1-positive nuclei were located inside the muscle basal laminae, which were visualized by immunofluorescence using anti-laminin antibody (Figs. 1B and C). This indicates that the nuclei of the myofibers are positive for Six1 in the adult skeletal muscle. Most of the Six1-positive nuclei were also positive for Six4 (Figs. 1D–F). In the regenerating TA muscle, the number of cells positive for Six1 was far greater than that of control TA muscle (Fig. 1I, compare to 1A). The Six1-positive cells in the regenerating TA muscle were located inside and outside the basal laminae (Figs. 1J and K). As observed in the control TA muscles, most of the cells positive for Six1 were also positive for Six4 in the regenerating TA muscle (Figs. 1L–N). It was noted that the relative intensities of immunofluorescent signals for Six1 and Six4 were more variable in the regenerating muscle (Fig. 1N), compared to those in the intact muscle (Fig. 1F). To determine the type of cells positive for Six1 and Six4, we examined the expression of MyoD, a marker of proliferating myogenic precursor cells and postmitotic myocytes in the regenerating muscle [28–30]. Triple immunofluorescence using anti-Six1, anti-Six4 and anti-MyoD antibodies revealed that most of the immunofluorescent signals of Six1 and Six4 were colocalized with that of MyoD (Figs. 1O and P). As shown in Fig. 1Q, $90.1 \pm 0.42\%$ of Six1-positive cells and $91.7 \pm 1.06\%$ of Six4-positive cells were colocalized with MyoD. Moreover, remarkable amounts of Six1 and Six4 immunofluorescent signals were positive for Ki67, a marker of proliferating cells, suggesting that substantial populations of Six1- and Six4-positive cells were mitotic (Figs. 1R–T, data not shown). Colocalization of Six1 and Six4 with MyoD was not observed in the control skeletal muscle (Figs. 1G and H). These findings indicate that (i) Six1 and Six4 are expressed both in normal and regenerating muscles and (ii) the number of cells positive for Six1 and Six4 robustly increases during regeneration of adult skeletal muscle and many of them are proliferating myogenic precursors.

Expression of Six proteins in muscle satellite cells

In the adult skeletal muscle, typical quiescent satellite cells can be recognized as mononuclear cells beneath the basal lamina, and these cells are positive for both Pax7 and M-cadherin [30–32]. To determine whether Six proteins are expressed in quiescent muscle satellite cells, we performed immunofluorescence studies for Six1, Pax7 and M-cadherin. Immunofluorescent signals of Pax7 (Fig. 2A) and M-cadherin (Fig. 2B) were observed in the mononuclear cells of adult TA muscle (Figs. 2A, B and E, arrowheads and insets). Six1 immunofluorescence signal was also observed in these cells

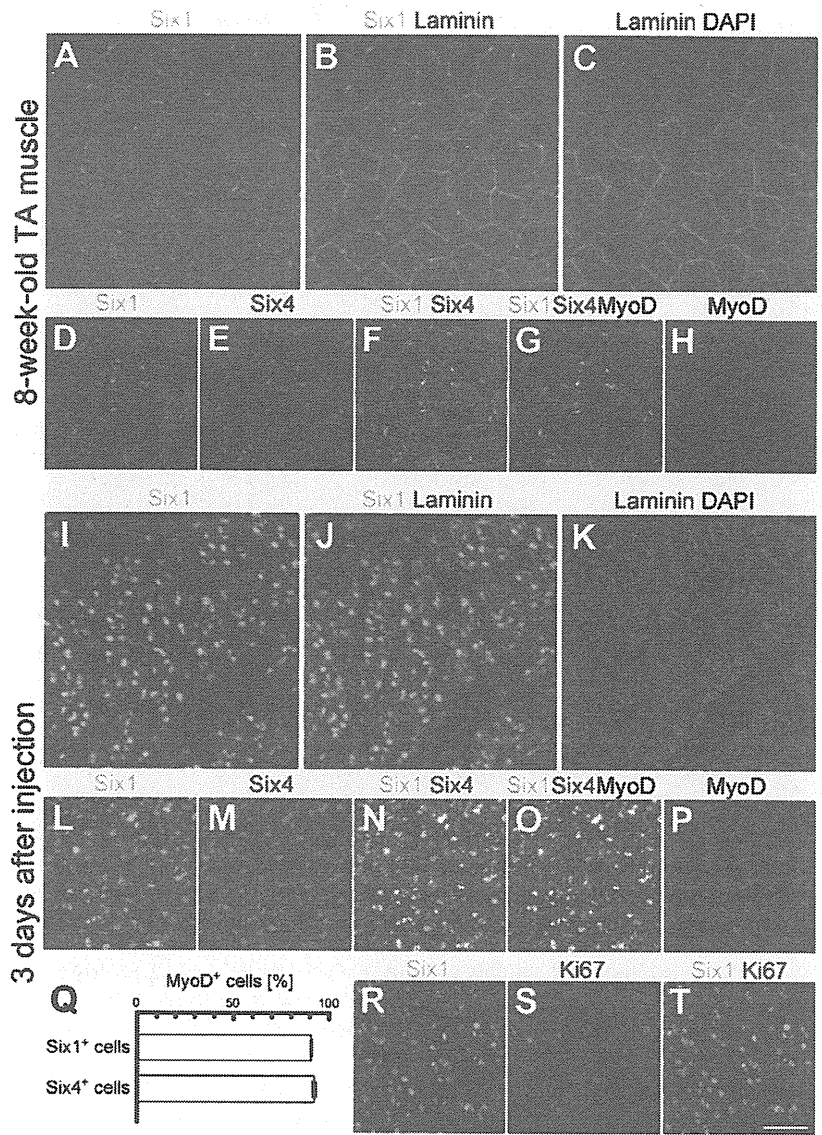

Fig. 1 – Expression of Six1 and Six4 in regenerating skeletal muscles of adult mice. (A–C) Cross-sections of intact TA muscle of 8-week-old mouse were stained with antibodies to Six1 (green) and laminin (red). Nuclei were stained with DAPI (blue). Note the subset of nuclei beneath the laminin layer is positive for Six1. (D–H) Immunofluorescence of cross-sections of TA muscle immunostained with antibodies for Six1 (green), Six4 (red) and MyoD (blue). Merged figures are shown in panels F and G. Most Six1-positive nuclei were positive for Six4 (E and F). MyoD was not detected in the adult TA muscle (H). (I–K) Cross-sections of regenerating TA muscle 3 days after cardiotoxin injection were co-immunostained with antibodies to Six1 (green) and laminin (red). Nuclei were stained with DAPI (blue). Note Six1-positive nuclei located inside and outside the laminin layer (J). (L–P) Immunofluorescence of cross-sections of regenerating TA muscle immunostained with antibodies for Six1 (green), Six4 (red) and MyoD (blue). Merged figures are shown in panels N and O. The majority of Six1-positive nuclei are also positive for Six4. Most of Six1- and Six4-positive nuclei are colocalized with MyoD. The percentages of MyoD-positive cells were quantified in (Q). Data are mean ± SEM. (R–T) Regenerating TA muscle immunostained with antibodies for Six1 (green) and Ki67 (red). A remarkable number of Six1-positive nuclei is positive for mitotic marker, Ki67. Scale bar: 50 μm.

(Figs. 2C and D, arrowheads and insets). The expression of Six4 was also observed in the satellite cells positive for M-cadherin in the adult TA muscle (Fig. 2F, thick arrow and inset). It is noteworthy that some of the nuclei within the myofibers, which were negative for Pax7 and M-cadherin, were positive for Six1 and Six4 (Figs. 2C–F arrows, data not shown). Vice versa, some of the Pax7 and M-cadherin-positive cells were negative for Six1 and Six4 (data not shown).

To examine the expression of Six proteins in muscle satellite cells during activation, proliferation and differentiation, we isolated and cultured satellite cells from limb and back muscles of wild-type mice by FACS technique using the monoclonal antibody SM/C-2.6 [4,5]

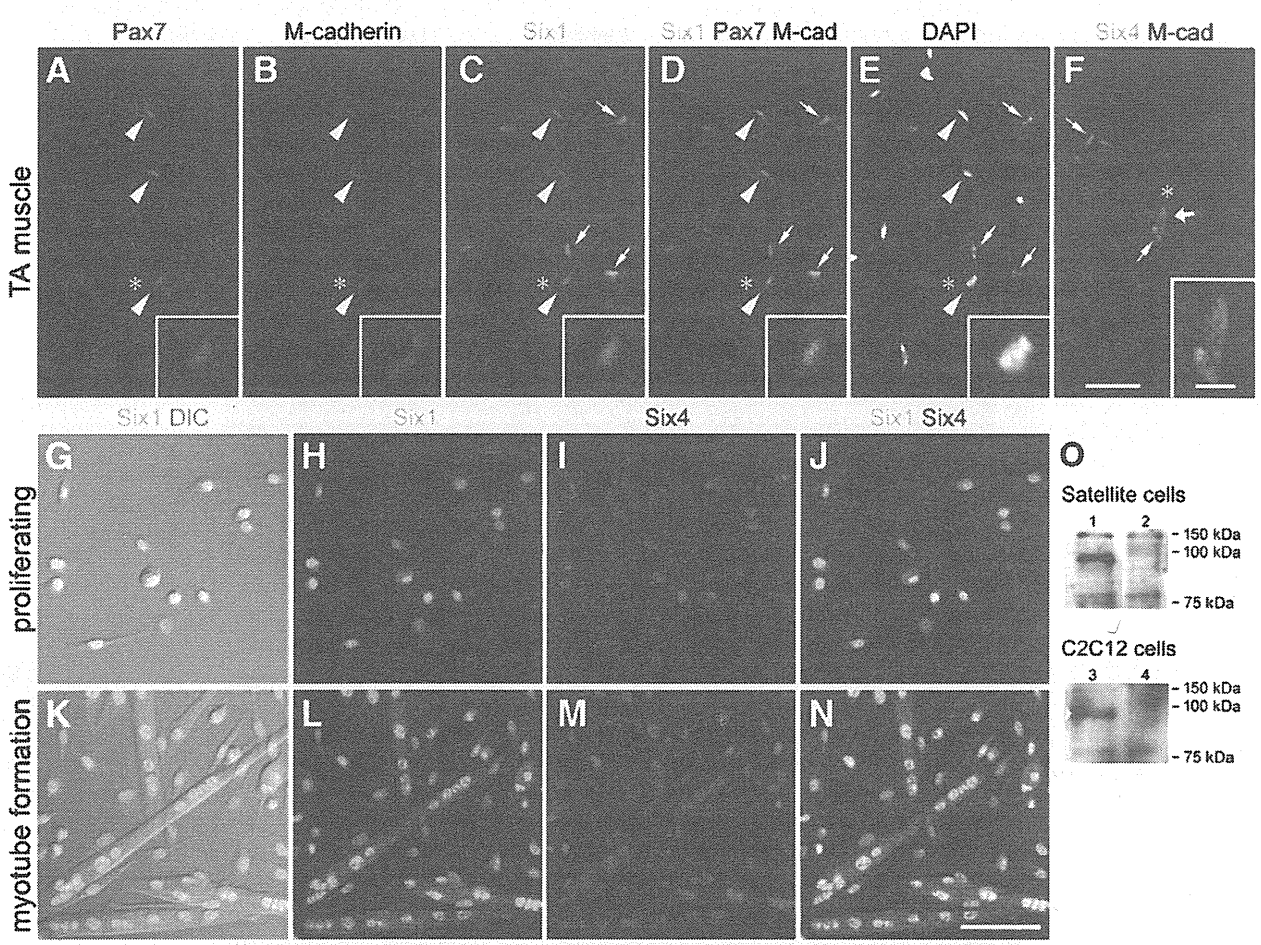

Fig. 2 – Six1, Six4 and Six5 are expressed in muscle satellite cells. (A–F) Cross-sections of TA muscle of 8-week-old mouse were immunostained with antibodies to Pax7 (red in A), M-cadherin (blue in B) and Six1 (green in C). Merged figures are shown in (D). The position of nuclei was visualized with DAPI, as shown in panel E. Satellite cells were labeled with the co-immunofluorescence of both Pax7 and M-cadherin (arrowheads). A subset of Six1-positive cells was satellite cells (C and D). A subset of Six4-positive cells was also labeled with M-cadherin (thick arrow in F). Arrows indicate myonuclei positive for Six1 or Six4 (C–F). Insets show close-up of satellite cells (labeled by asterisk). (G–N) Immunofluorescence of SM/C-2.6-positive satellite cells in the growth medium (G–J) or in the differentiation medium (K–N) using antibodies to Six1 (G, H, K and L in green) and Six4 (I and M in red). Merged figures are shown in panels J and N. Differential interference contrast (DIC) image showed that the majority of satellite cells were mononuclear fibroblastic cells in the growth medium (G) or formed multinucleated myotubes in the differentiation medium (K). Cultured satellite cells were positive for both Six1 and Six4 (J and N). Scale bars: 20 μm (A–F), 5 μm (insets) and 100 μm (G–N). (O) Nuclear (lane 1) and cytoplasmic (lane 2) extracts from SM/C-2.6-positive satellite cells were analyzed by western blotting with anti-Six5 antibody. For reference, nuclear (lane 3) and cytoplasmic (lane 4) extracts were also prepared from C2C12 cells and analyzed. Arrowheads indicate the positions of the detected Six5 proteins. The position of molecular mass marker is shown on the right.

and used immunofluorescence staining to check for the presence of Six1 and Six4. Six1 immunofluorescence was observed in virtually all muscle satellite cells in the growth medium (Figs. 2G and H). Six4 immunofluorescence was also observed in these satellite cells (Fig. 2I). Although Six1 and Six4 were colocalized in almost all satellite cells, the relative immunofluorescence intensity and subcellular distribution of Six1 and Six4 varied among individual cells (Fig. 2J). To examine whether Six1 and Six4 proteins are present during differentiation, the isolated satellite cells were cultured in the differentiation medium. Most of the satellite cells formed myotubes within 24 hours (Fig. 2K). Myonuclei in the myotubes were positive for Six1 (Figs. 2K and L) and Six4 (Fig. 2M), though the relative immunofluorescence intensities varied among myonuclei (Fig. 2N), as observed in the growth medium (Fig. 2J). We investigated the presence of Six5 in satellite cells by western blotting (Fig. 2O). Nuclear and cytoplasmic extracts from muscle satellite cells cultured in the growth medium were prepared and analyzed by western blotting using anti-Six5 antibody. Six5 protein was detected in nuclear extracts (Fig. 2O lane 1) but not in the cytoplasmic extracts (Fig. 2O lane 2). Furthermore, Six5 protein was detected in nuclear extracts only, but not cytoplasmic extracts, prepared from the control C2C12 mouse myoblast cell (Fig. 2O, lanes 3 and 4, respectively). These results indicate the presence of Six proteins mainly in the nuclei of quiescent, proliferating and differentiating muscle satellite cells.

Overexpression of Six genes inhibits proliferation of muscle satellite cells

Having shown that Six proteins are expressed in quiescent, proliferating and differentiating muscle satellite cells, we next investigated the effects of overexpression of *Six1* as well as *Six4* and *Six5* in isolated muscle satellite cells. In these studies, a retrovirus-mediated system [33] was used to overproduce Six1, Six4 and Six5 proteins. Six proteins and EGFP were connected by IRES. EGFP fluorescence was used to monitor cells transduced with the recombinant retrovirus. Accumulation of Six1, Six4 and Six5 proteins was noted in the nuclei of EGFP-positive cells after infection with a retrovirus harboring *Six1*, *Six4* or *Six5* cDNA, respectively (Supplementary Fig. 1). The nuclear localization was similar to the endogenous Six proteins both *in vivo* and *in vitro* (Figs. 1 and 2).

To analyze the effects of overexpression of *Six* genes on cell proliferation, we assessed the expression of proliferation markers, phospho-histone H3 and Ki67, by immunofluorescence (Fig. 3). Among the cells infected with the control retrovirus, a subset of EGFP-expressing cells was positive for phospho-histone H3 (Fig. 3A, arrowheads). In contrast, the signal of phospho-histone H3 was rarely observed in EGFP-positive cells infected with a retrovirus harboring *Six1*, *Six4* or *Six5* cDNA (Figs. 3B–D). Immunofluorescence of Ki67 was also observed in EGFP-positive cells infected with the control virus (Fig. 3E, arrowheads), but rarely in EGFP-positive cells infected with the retrovirus harboring *Six1*, *Six4* or *Six5* cDNA (Figs. 3F–H). To quantify cell proliferation, we determined the percentage of Ki67-positive cells among the EGFP-positive cells (Fig. 3I). The Ki67 index was $15.1 \pm 2.2\%$ in control, but significantly reduced to $5.7 \pm 1.4\%$, $4.8 \pm 1.9\%$ and $5.4 \pm 1.3\%$ in cells infected with retrovirus harboring *Six1*, *Six4* and *Six5*, respectively, indicating that overproduction of these Six proteins suppresses the proliferation of satellite cells.

Overexpression of Six1 promotes and excess Six4 and Six5 repress differentiation of muscle satellite cells

To investigate the effects of *Six* gene overexpression on the differentiation of muscle satellite cells, these cells were cultures in differentiation medium after retrovirus infection. EGFP signals were detected in myotubes and scattered mononuclear cells in the control experiment (Fig. 4A). Infection of the satellite cells with a retrovirus harboring *Six1* resulted in a considerable increase in the size of EGFP-positive myotubes relative to the control (Fig. 4B). On the other hand, many scattered single cells were positive for EGFP and fewer myotubes were observed when the retrovirus harboring *Six4* or *Six5* was used for infection (Figs. 4C and D). To assess cell differentiation, the fusion index of EGFP-positive cells (see Materials and methods) and the mean number of nuclei in EGFP/skeletal muscle myosin-double positive cells were determined after viral infection (Figs. 4E and F). The fusion index was $63.9 \pm 3.62\%$ in cells infected with the control retrovirus, and significantly higher ($82.3 \pm 2.39\%$) in cells infected with the retrovirus harboring *Six1* (Fig. 4E). In contrast, the index was $15.0 \pm 3.19\%$ and $13.8 \pm 2.72\%$ in Six4- and Six5-overexpressing cells, respectively; the latter values were significantly lower than the control. The mean number of nuclei in myosin-positive cells was 2.30 ± 0.20 when the control virus was used for infection (Fig. 4F), but increased to 3.82 ± 0.39 in cells infected with retrovirus harboring *Six1*, and decreased to 1.18 ± 0.06 and 1.16 ± 0.05 by infection with retrovirus overexpressing *Six4* and *Six5*, respectively. These results indicate that overproduction of Six1 stimulates while that of Six4 or Six5 inhibits the differentiation of muscle satellite cells in the differentiation medium.

To confirm the above effects of *Six* genes overexpression on satellite cell differentiation, the fusion index of EGFP-positive cells and the mean number of nuclei in myosin-positive cells were determined in the growth medium (Fig. 4G and H). The fusion

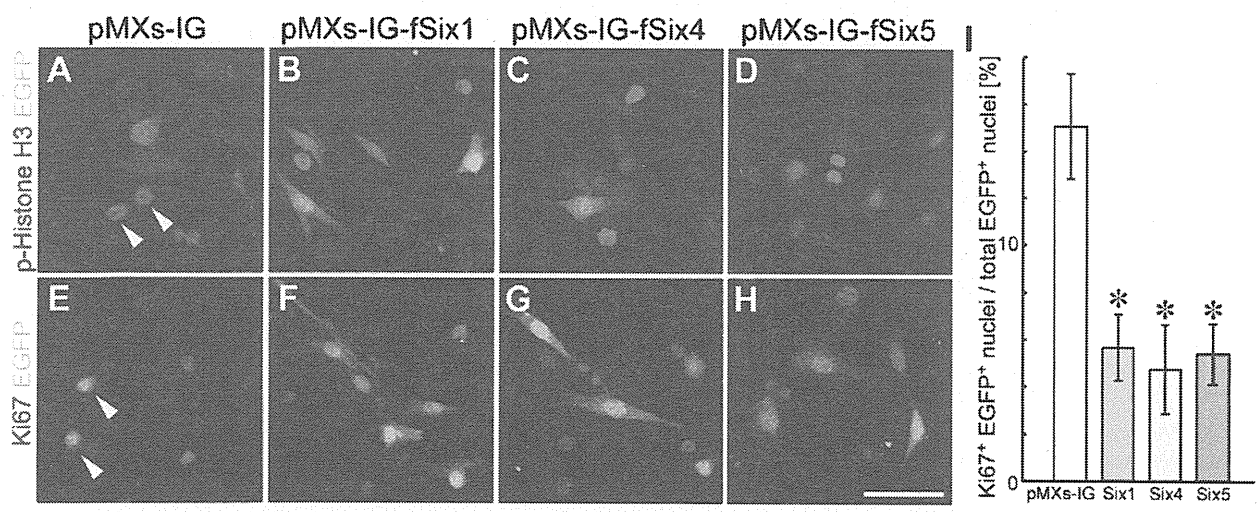

Fig. 3 – Overproduction of Six1, Six4 and Six5 interferes with proliferation of muscle satellite cells. Immunofluorescence of satellite cells infected with control retrovirus (A and E) or retrovirus harboring *Six1* (B and F), *Six4* (C and G) or *Six5* (D and H) in the growth medium using antibodies to phospho-histone H3 (A–D) or Ki67 (E–H), shown in red. Arrowheads point to EGFP-positive cells immunostained with anti-phospho-histone H3 (A) or anti-Ki67 (E) antibodies. Scale bar: 50 μm. (I) The percentages of Ki67-positive nuclei among EGFP-positive cells infected with control retrovirus (pMXs-IG) and retrovirus harboring *Six1* (Six1), *Six4* (Six4) or *Six5* (Six5) were calculated. Data are mean ± SEM of three independent cell isolates. *$p < 0.001$, compared with pMXs-IG.

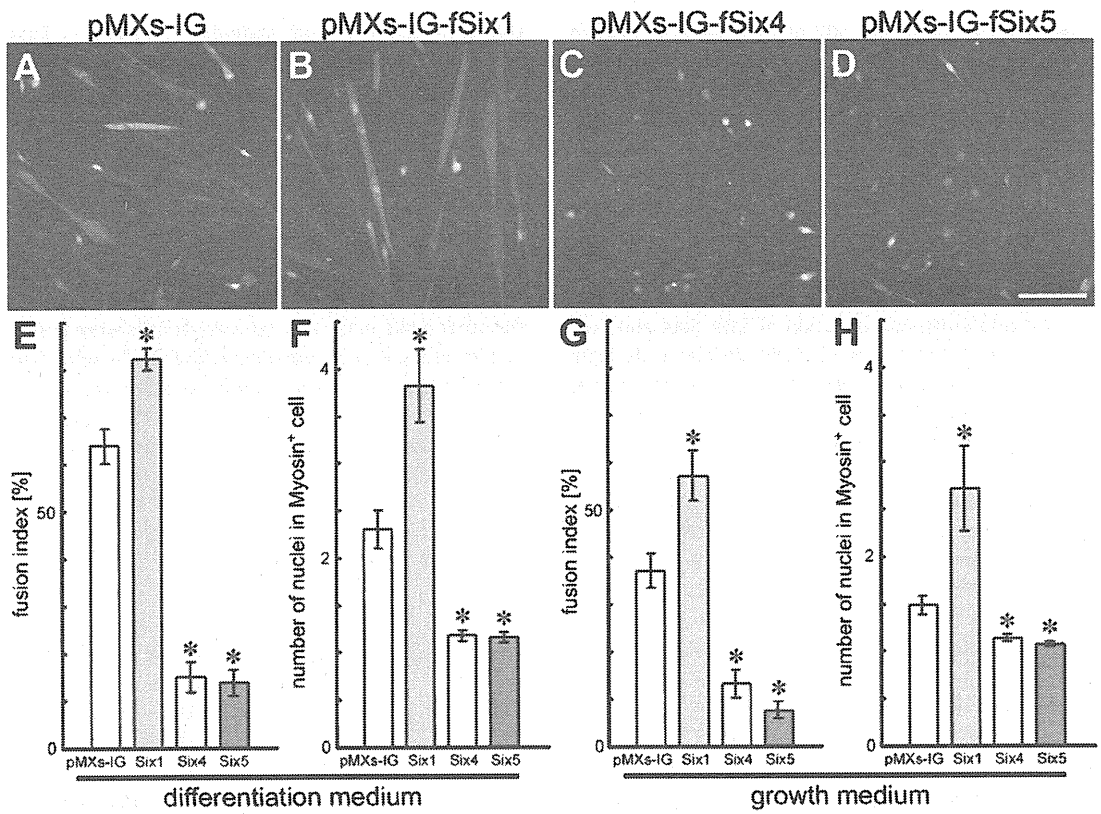

Fig. 4 – Effects of overproduction of Six1, Six4 and Six5 on differentiation of muscle satellite cells. Representative images of EGFP-positive cells infected with control retrovirus (A) and retrovirus harboring *Six1* (B), *Six4* (C) or *Six5* (D) in the differentiation medium. Nuclei were stained with DAPI (blue). Scale bar: 100 μm. The percentage of nuclei within myotubes (fusion index) was calculated among the EGFP-positive cells (E and G) and the number of nuclei in EGFP and skeletal muscle myosin-double positive cells was counted and averaged (F and H) in the differentiation medium or growth medium, respectively, following infection with control retrovirus (pMXs-IG) or retrovirus harboring *Six1* (Six1), *Six4* (Six4) or *Six5* (Six5). Data are mean ± SEM of three independent cell isolates. *$p < 0.001$, compared with pMXs-IG.

index was 37.2 ± 3.73% and the mean number of nuclei in myosin-positive cells was 1.48 ± 0.10 in cells infected with the control retrovirus (Figs. 4G and H, pMXs-IG). These observations clearly indicate that differentiation occurs in a subset of satellite cells even in the growth medium, although the extent of differentiation is lower than that in the differentiation medium. Infection with a retrovirus harboring *Six1* increased the fusion index to 57.3 ± 5.35% as well as the mean number of nuclei in myosin-positive cells to 2.72 ± 0.45. On the other hand, in cells infected with retrovirus harboring *Six4* or *Six5*, the fusion index and mean number of nuclei in myosin-positive cells were reduced to 13.3 ± 2.93% or 7.57 ± 1.77% and 1.14 ± 0.04 or 1.07 ± 0.02, respectively (Figs. 4G and H). These results indicate that even in the growth medium, overproduction of Six1 promotes differentiation, whereas overproduction of Six4 or Six5 represses differentiation of muscle satellite cells.

Overproduction of Six4 or Six5 inhibits differentiation of satellite cells by down-regulation of myogenin expression

To determine the mechanism of Six1-induced enhancement and Six4-/Six5-induced inhibition of differentiation of satellite cells, we investigated the expression of key regulators of muscle differentiation and regeneration (Fig. 5).

Myogenin is expressed in myoblasts and plays an important role in muscle development [34,35] and its expression is positively controlled by *Six* genes [21,26,27]. The percentage of myogenin-positive cells in EGFP-positive satellite cells infected with the control retrovirus was 18.9 ± 1.68% (Figs. 5A, E, arrows and Q). Overexpression of *Six1* significantly increased the number of myogenin-positive cells to 27.5 ± 3.33% of EGFP-positive cells (Figs. 5B, F, arrows and Q). In contrast, the percentages of myogenin-positive cells were significantly reduced to 4.18 ± 1.71% and 2.49 ± 1.11% in satellite cells infected with the retrovirus harboring *Six4* and *Six5*, respectively (Figs. 5C, D, G, H, arrowheads and Q). These data suggest that misexpression of *Six1* promotes the expression of myogenin, whereas overexpression of *Six4* and *Six5* results in down-regulation of myogenin.

To investigate the effects of overproduction of Six proteins on the activation of muscle satellite cells, we analyzed the expression of MyoD and Pax7. Damage or injury of the skeletal muscle activates quiescent satellite cells as evident by coexpression of MyoD and Pax7 [3]. Following the induction of MyoD and Pax7 expression, most satellite cells undergo proliferation. Infection of satellite cells with the

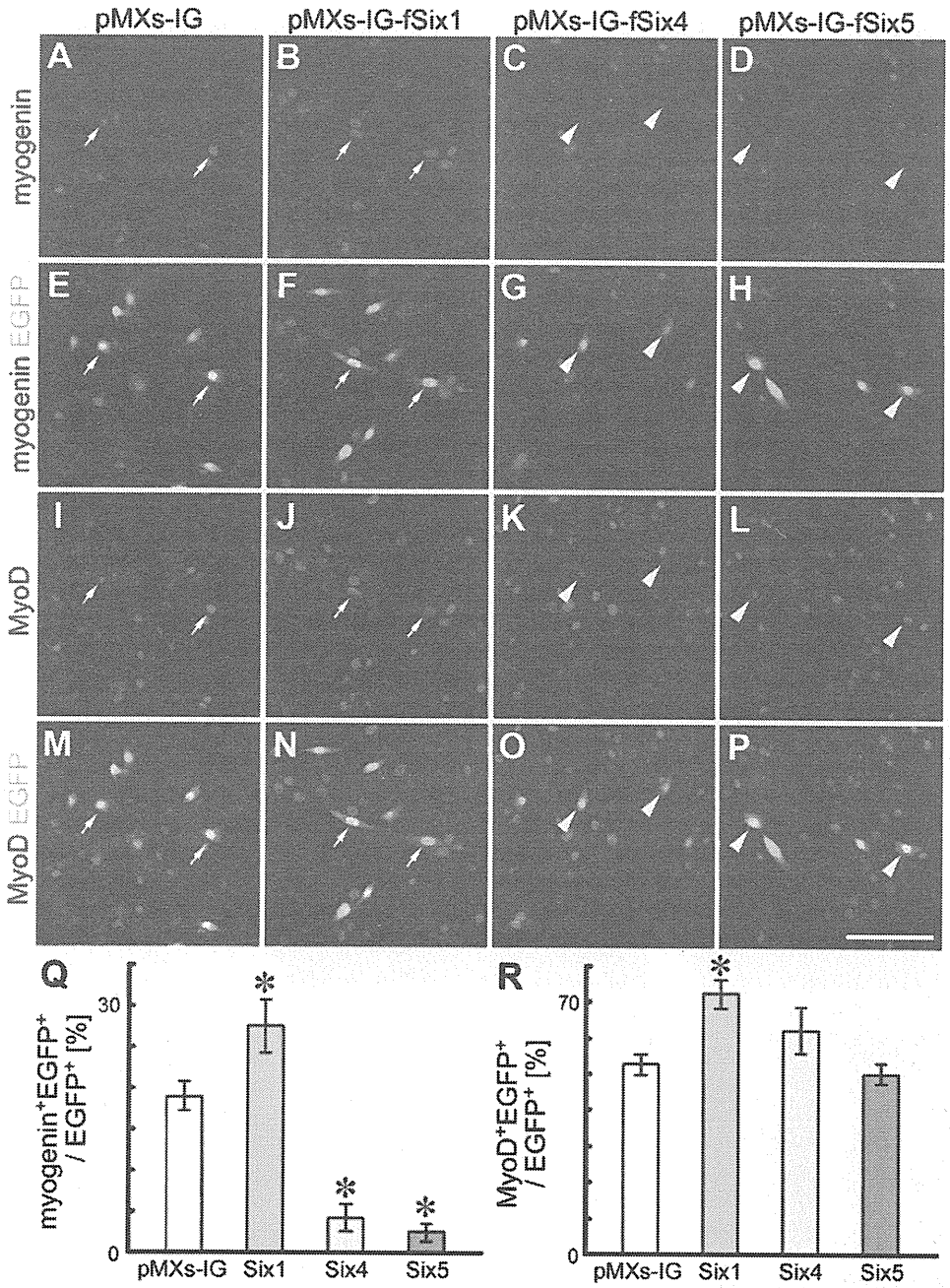

Fig. 5 – Effects of overproduction of Six proteins on the expression of myogenin and MyoD in muscle satellite cells. Immunofluorescence of satellite cells infected with control retrovirus (A, E, I and M) or retrovirus harboring *Six1* (B, F, J and N), *Six4* (C, G, K and O) or *Six5* (D, H, L and P) in growth medium using antibodies to myogenin (A–H in red) and MyoD (I–P in red). Arrows show colocalization of myogenin, MyoD and EGFP. Arrowheads point to weak signals of myogenin immunofluorescence in MyoD and EGFP-positive cells. Scale bar: 100 μm. The percentages of myogenin- and MyoD-positive cells were calculated among the EGFP-positive cells (Q and R). Data are mean ± SEM calculated from three similar results obtained from two independent cell isolates. *$p < 0.05$, compared with pMXs-IG.

control retrovirus resulted in the appearance of MyoD immunofluorescence in the nuclei of 53.9 ± 5.04% of EGFP-positive cells (Figs. 5I, M, arrows and R). The percentages of MyoD-positive cells increased significantly to 72.2 ± 3.95% with retrovirus harboring *Six1* (Figs. 5J, N, arrows and R), but only to 61.8 ± 6.45% and 50.0 ± 2.97% with retroviruses harboring *Six4* and *Six5*, respectively, which were not statistically different from that of the control (Figs. 5K, L, O, P, arrowheads and R). Cultured muscle satellite cells also expressed Pax7 (data not shown). The percentages of Pax7-positive cells were not apparently altered by the infections of retroviruses harboring any of the *Six* genes, compared with the control retrovirus (data not shown). The above results indicate that overexpression of *Six4* and